AGU PUBLICATIONS

JGR

Journal of Geophysical Research: Solid Earth

RESEARCH ARTICLE
10.1002/2015JB012565

Key Points:
- At least six earthquake events over the last 3 kyr have ruptured the Pizzalto fault
- Rare earth elements can be used to recover past events on a fault plane
- Earthquakes rupturing the Rotella-Aremogna fault system are clustered in time

Supporting Information:
- Supporting Information S1

Correspondence to:
J. Tesson,
tesson@cerege.fr

Citation:
Tesson, J., B. Pace, L. Benedetti, F. Visini, M. Delli Rocioli, M. Arnold, G. Aumaître, D. L. Bourlès, and K. Keddadouche (2016), Seismic slip history of the Pizzalto fault (central Apennines, Italy) using in situ-produced ^{36}Cl cosmic ray exposure dating and rare earth element concentrations, *J. Geophys. Res. Solid Earth*, *121*, doi:10.1002/2015JB012565.

Received 29 SEP 2015
Accepted 1 MAR 2015
Accepted article online 9 MAR 2016

Seismic slip history of the Pizzalto fault (central Apennines, Italy) using in situ-produced ^{36}Cl cosmic ray exposure dating and rare earth element concentrations

J. Tesson[1], B. Pace[2], L. Benedetti[1], F. Visini[3], M. Delli Rocioli[2], M. Arnold[1], G. Aumaître[1], D. L. Bourlès[1], and K. Keddadouche[1]

[1]Aix-Marseille Université, CNRS, IRD, CEREGE UM34, Aix-en-Provence, France, [2]DiSPUTer, Università "G. d'Annunzio" Chieti-Pescara, Chieti Scalo, Italy, [3]Istituto Nazionale di Geofisica e Vulcanologia, L'Aquila, Italy

Abstract Morphological and geological observations reveal that most Apenninic faults are highly segmented and that the majority of the fault segments are less than 10 km long. Although these faults have undergone numerous paleoseismological investigations, quantitative data remain crucially lacking for a large number of fault segments. Because such data are essential to understanding how these faults have ruptured and interacted in the past and how they might behave in the future, we investigated the Holocene seismic history of the Pizzalto normal fault, a 13 km long fault segment belonging to the Pizzalto-Rotella-Aremogna fault system in the Apennines. We collected 44 samples from the Pizzalto fault plane exhumed during the Holocene and analyzed the ^{36}Cl and rare earth element (REE) contents. Together, the ^{36}Cl and REE concentrations show that at least six events have exhumed 4.4 m of the fault scarp between 3 and 1 ka, with slip per event values ranging from 0.3 to 1.2 m. No major events have been detected over the last 1 kyr. The Rotella-Aremogna-Pizzalto fault system has a clustered earthquake behavior with a mean recurrence time of 1.2 kyr and a low to moderate probability (ranging from 4% to 26%) of earthquake occurrence over the next 50 years.

1. Introduction

The magnitude and recurrence interval of past earthquakes on a fault and the fault geometry are the main input parameters for probabilistic and deterministic fault-based seismic hazard assessments [*Peruzza et al*., 1997; *Pace et al*., 2006; *Field et al*., 2014, 2015]. The mean interseismic period or the mean slip rate is generally used as input data in those models to assess the activity of a fault. However, how can the recurrence interval be accurately determined on a single fault? An increasing number of data sets have shown that earthquakes on faults do not repeat regularly and instead exhibit alternating periods of intense seismic activity and long periods of quiescence [*Wallace*, 1987; *Friedrich et al*., 2003; *Benedetti et al*., 2013]. It is therefore essential to acquire paleoseismological records long enough to capture the full seismic cycle [*Weldon et al*., 2004; *Schlagenhauf et al*., 2011; *Mouslopoulou et al*., 2012] to be able to accurately describe the seismogenic potential of a fault.

In Italy, and particularly in the central Apennines, several large earthquakes (M_w 6–7) have occurred over the last thousand years. The focal mechanisms of instrumented $M > 5$ earthquakes show that those earthquakes have occurred mainly along normal faults (Colfiorito 1998 M_w 6.0; L'Aquila 2009 *M*w 6.2). Such earthquakes produce surface ruptures that are 15–20 km in length and have surface coseismic offsets of ~20 cm (L'Aquila case [*Boncio et al*., 2010]) to 1 m (Fucino case [*Serva et al*., 1989]).

Morphological and geological observations reveal that most faults are segmented at the surface and that the majority are less than 10 km long. For example, several scientists [*Boncio et al*., 2010; *Pucci et al*., 2015; *Civico et al*., 2015] showed that the L'Aquila basin is affected by small (less than 5 to 10 km long) normal fault segments that mostly dip westward and trend NW-SE. These observations have suggested that earthquakes in Italy can rupture multiple segments belonging to larger fault systems. In fact, multiple triggering, with variable time delays, has been observed in several damaging earthquake sequences in the Italian Apennine belt. For example, the 2009 L'Aquila M_w 6.3 earthquake was followed, a day after, by an M_w 5.6 event at the southeast edge of the main fault. The seismicity of the whole sequence spread over a 40 km long fault system [*Chiarabba et al*., 2009]. The 1997–1998 Umbria-Marche seismic sequence was characterized by three main shocks in 1 month, with two main shocks breaking adjacent parts of the two faults within a few

hours of each other [*Chiaraluce et al*., 2005]. Overall, this sequence numbered six shocks of moderate magnitude ($5.2 \leq M_w \leq 6.0$), occurring along a 40 km long fault system. The 1984 Barrea earthquake [*Pace et al*., 2002] ruptured at least three 5 km long segments. Finally, the 1980 M_w 6.9 Irpinia earthquake was composed of a sequence of three distinct subevents, nucleating on different faults at time intervals of approximately 20 s [*Pingue et al*., 1993; *Troise et al*., 1998].

During the last 30 years, paleoseismology and structural geology investigations have provided key data for fault-based probabilistic seismic hazard models [e.g., *Peruzza et al*., 2011] and have significantly enhanced our knowledge on the seismic potential of these active faults. However, fault-based probabilistic seismic hazard modeling requires a model for the seismogenic source, which is defined as a continuous structure in length and at depth, even when the surface observations clearly show segmentation with closely spaced fault segments of minor hierarchical order. The along-strike segmentation of faults significantly controls the rupture length, slip distribution, and the resulting magnitude of an earthquake [*Manighetti et al*., 2007; *Kase*, 2010; *Manighetti et al*., 2015; *Pace et al*., 2016]. For example, geometrical criteria, such as fault gaps among aligned structures, sharp bends, or intersections, have been used in *Peruzza et al*. [2011] to define the along-strike segmentation of seismogenic faults in Central Italy. It is thus important to be able to better define the occurrence of events on smaller segments belonging to a larger fault system, which up to now remains poorly studied.

To better assess how earthquakes can affect the central Apennines in the future, it is essential to acquire accurate data on their seismic history on a time scale long enough to capture the entire seismic cycle. A key observation is that the cumulative effect of earthquakes over 10^4 years timescale has been preserved because the rate of vertical offset of the ground surface across faults is higher than the erosion and sedimentation rates since the last glacial maximum (12–18 ka [*Giraudi*, 1995; *Roberts and Michetti*, 2004, *Papanikolaou and Roberts*, 2007]). Under the hypothesis that coseismic processes dominate the exhumation of a fault plane, cosmogenic nuclide analysis has provided a new tool to recover the Holocene seismic activity of a fault [*Mitchell et al*., 2001; *Palumbo et al*., 2004; *Schlagenhauf et al*., 2010]. This methodology has been successfully used in the Apennines. It provides new paleoseismological data in places where the classical trenching approach is not applicable and reveals a more complete and complex picture of Apenninic normal fault seismicity over the last 20 kyr, such as clustered events and apparent fault interactions [*Benedetti et al*., 2013].

Assessing the Holocene seismic history of each fault segment is an immense task that is nevertheless necessary to improve our knowledge of how these faults have ruptured and interacted in the past and how they might behave in the future. In this framework, we focus here on the 13 km long Pizzalto fault located at the southern tip of the Sulmona Basin. This area has not been affected by major earthquakes over the last 300 years (since the 1706 Maiella earthquake) and is located southeast of the L'Aquila fault system. Using ^{36}Cl cosmic ray exposure dating combined with rare earth element (REE) concentrations of samples from the fault plane, the exhumation history of the 10 m high limestone bedrock fault plane is investigated. Both data sets lead to a seismic scenario suggesting that this fault has been seismically active over the last 3 kyr. Existing paleoseismological data from the adjacent Aremogna-Cinque Miglia fault system are compared with this new record. The results are then used to update the fault-based earthquake rupture forecast for the next 50 years in this region.

2. Seismotectonic Context of the Pizzalto Fault

The central Apennines, and in particular the Abruzzo region, belongs to a mountain belt initially shaped by a SW-NE late Miocene-early Pliocene compressional phase associated with the formation of the NE verging fold-and-thrust structures in primarily carbonate rocks (e.g., the Gran Sasso range, Maiella range, Marsica-Morro range, and Velino-Magnola range). Since the late Pliocene-early Pleistocene, SW-NE extension has dominated the active tectonics of the area, with ongoing motion on normal faults [e.g., *Lavecchia et al*., 1994; *Benedetti*, 1999; *Piccardi et al*., 1999; *Roberts and Michetti*, 2004].

Ongoing motion on normal faults has long been recognized from the identification of geomorphic features commonly observed on normal faults worldwide [e.g., *Wallace*, 1977; *Armijo et al*., 1986; *Armijo et al*., 1992], such as continuous, concave, 50–300 m high triangular facets with perched valleys, attesting to long-term motion (10^4–10^5 yr). Recent postglacial activity is often highlighted by the presence of steep several-meter-high scarplets preserved at the base of these cumulative escarpments. While such geomorphic features are observed along most of the normal faults recognized in the Abruzzo region [*Bosi*, 1975; *Piccardi et al*., 1999; *Benedetti et al*., 2013], additional evidence of an ongoing extension in the Apennines is also

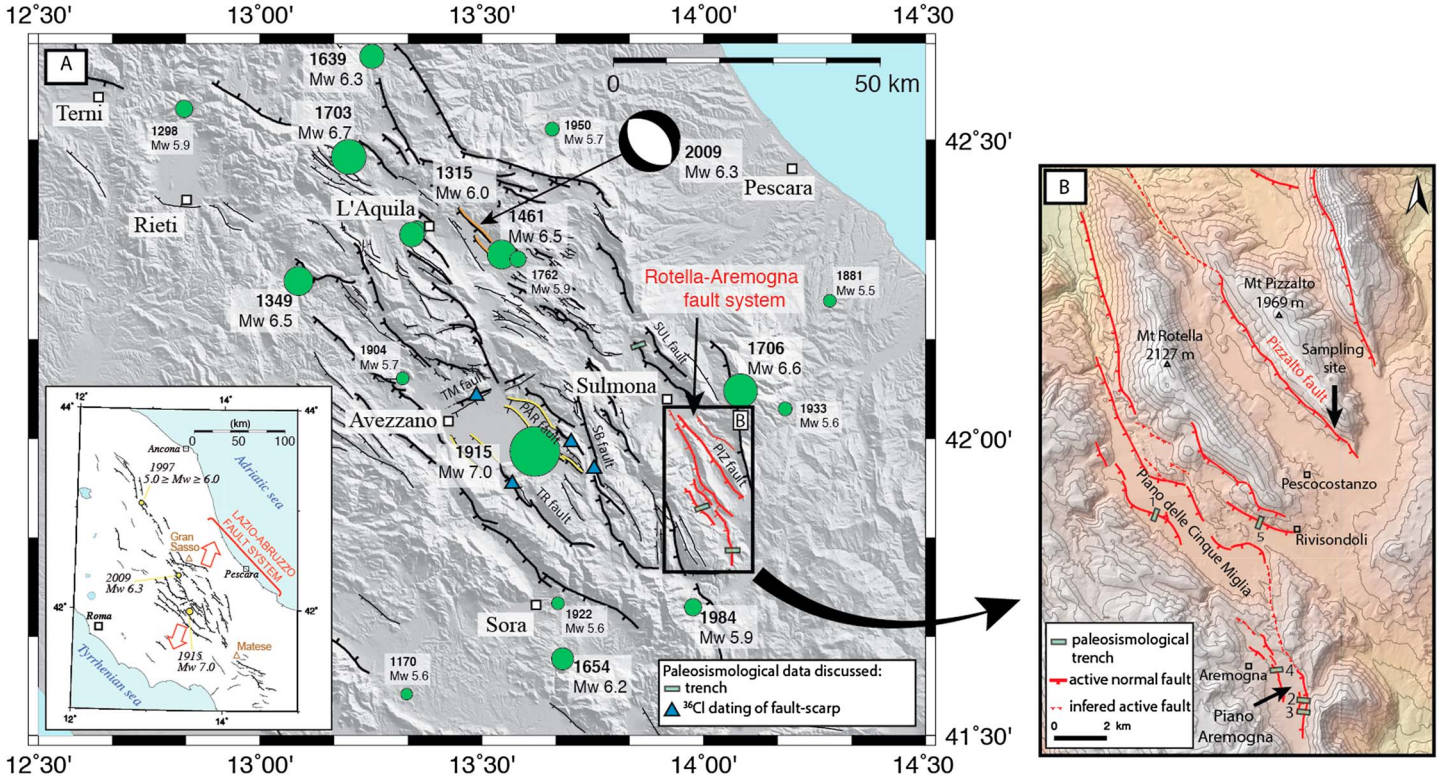

Figure 1. (a) Seismotectonic map of the Lazio-Abruzzo fault system. Active normal faults in black are from *Benedetti et al.* [2013]. Shaded relief from the 90 m pixel Shuttle Radar Topography Mission digital elevation model. Historical earthquake epicenters in green ($M_w \geq 5.9$) are from the CPTI11 catalogue [*Rovida et al.*, 2011] that covers the time period of 1005–2006. Faults that ruptured during the 1915 and 2009 earthquakes are underlined in yellow and orange, respectively. The location of published paleoseismological data discussed in this paper are represented by green rectangles for trench sites (1, 2, 3 for *D'addezio et al.* [2001], 4 for *Frezzotti and Giraudi* [1989], and 5 for *Brunamonte et al.* [1991]) and by blue triangles for ^{36}Cl fault plane exposure dating sites [*Benedetti et al.*, 2013]. PIZ, Pizzalto fault; SUL, Sulmona fault; TM, Tre-Monti fault; TR, Trasacco fault; SB, San Sebastiano fault; and PAR, Parasano fault. (a) Seismotectonic map of the Pizzalto-Rotella-Aremogna fault system. Shaded relief from the 10 m pixel TINITALY/01 digital elevation model [*Tarquini et al.*, 2007]. The Cinque-Miglia and Aremogna active faults have been vectorized from *D'Addezio et al.* [2001].

provided by field geology and paleoseismology [e.g., *Galadini and Galli*, 2000; *Bosi et al.*, 2003; *Galli et al.*, 2008], geodetic data [e.g., *D'Agostino et al.*, 2008], focal mechanisms [e.g., *Pondrelli et al.*, 2006], and seismotectonic studies [e.g., *Pace et al.*, 2002; *Boncio et al.*, 2004].

The active normal faults in the Apennines strike parallel to the mountain belt axis, on average NW-SE, and generally dip to the SW (Figure 1). The Pizzalto fault, located approximately 50 km southeast of the epicenter of L'Aquila 2009 earthquake, is ~12 km long, trends NNW, and dips SW (Figure 1). It belongs to a larger-scale fault system, the 30 km long Rotella-Aremogna active normal fault system (Figure 1) [*Boncio et al.*, 2004; *Benedetti et al.*, 2013].

The Pizzalto fault segment, which bounds the eastern side of Mount Pizzalto (1966 m above sea level), is the easternmost segment of the Rotella-Aremogna fault system. The trace of the fault is highlighted on the digital shaded relief model (Figure 2a) by a sharp slope break and incised rivers stopping at midrelief with small surfaces at the base. On the other side of the valley, the morphological expression of the relief is very different and features a generally concave slope and rivers that incise similarly through the various slope breaks and the topography (Figure 2c). Moreover, the trace of the fault is outlined by a fresh, very well preserved, continuous, linear 0.2 to 10 m high limestone fault scarp visible in the field above the small surfaces (Figure 2d).

The hanging wall of the fault is made of a thick colluvial wedge (several tens of meters thick, based on field outcrops) (Figures 3a and S1). At least two layers of colluvial deposits have been identified and mapped mainly based on field observations [*Miccadei and Parotto*, 1998; *Bosi et al.*, 2003]. The overlying outcropping deposits are noncemented limestone slope breccia that dip gently southwestward and most likely originate from the slope of Mount Pizzalto (Figure 3). These deposits rest on an older subhorizontal cemented slope breccia assigned to the middle-upper Pleistocene [*Bosi et al.*, 2003]. There are some small local variations

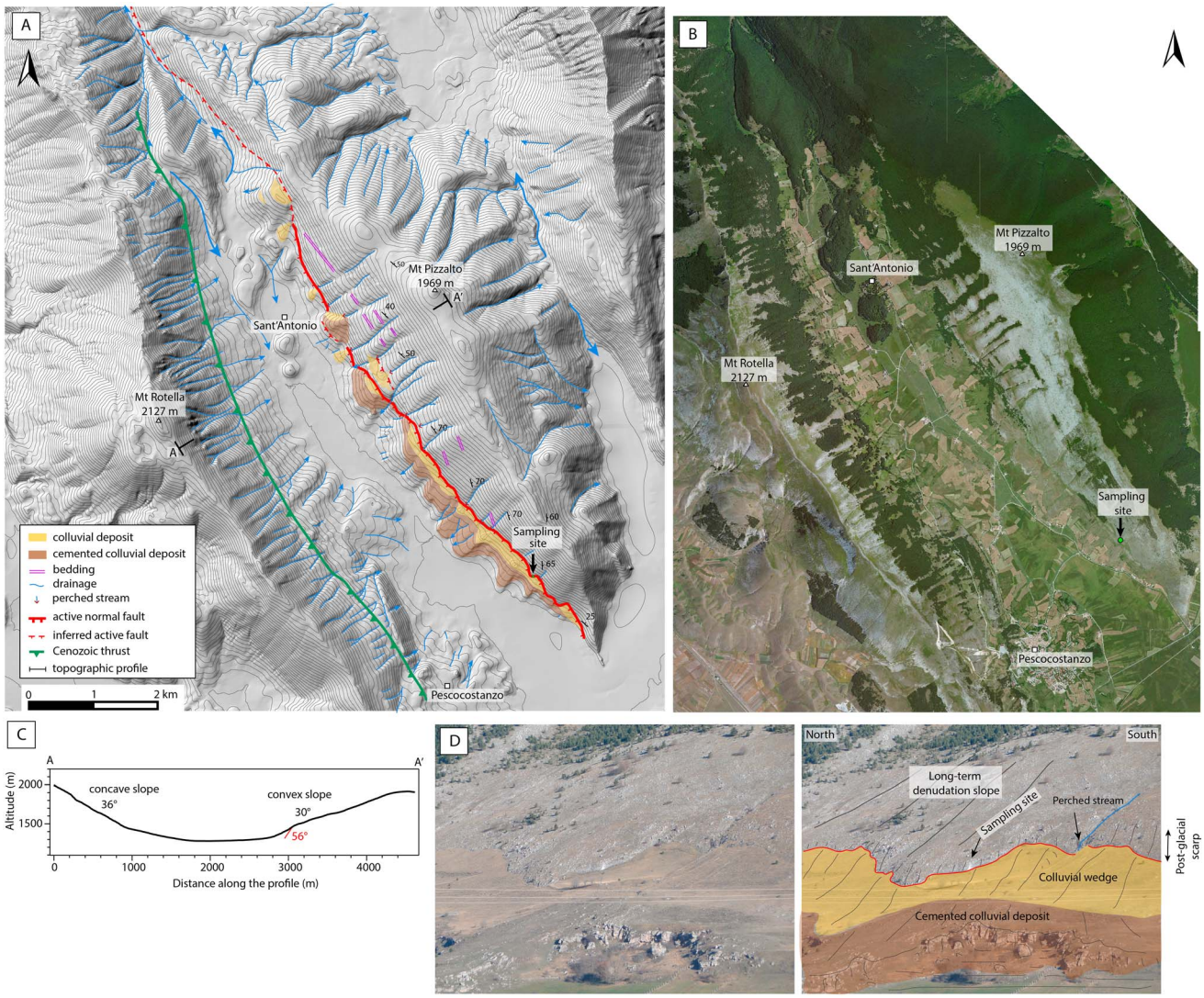

Figure 2. Morphotectonic analysis: (a) Morphotectonic map of the Pizzalto fault using shaded relief from a 5 m pixel digital elevation model. Isoaltitude contours represent every 20 m. (b) Photomosaic from Bing imagery showing the fresh trace of the Pizzalto fault. (c) Topographic profile from Mount Rotella (A) to Mount Pizzalto (A') highlighting the morphological differences between the concave slope of Mount Rotella, which is not affected by an active fault, and the convex slope of Mount Pizzalto, which is apparently the result of activity on the Pizzalto fault. (d) Interpretative photo of sampling site morphology.

in the dip of these colluvial deposits that are most likely due to slope readjustments and gravitational movements prior to the cementation (Figure S1). In contrast, the upper and most recent layers of those deposits homogeneously dip 10–20° southwestward, suggesting no recent gravitational movement (Figure S1).

Past large earthquakes associated with the Rotella-Aremogna fault system have been previously studied by several scientists (see trench locations in Figure 1b). *D'Addezio et al.* [2001] identified three events occurring at approximately 7–6 ka, 6–5 ka, and 3–1 ka in paleoseismological trenches performed on the Aremogna-Cinque Miglia fault, at the southern tip of the fault system. *Brunamonte et al.* [1991] suggest that one seismic event might have occurred at less than 4.3 ka. *Galli et al.* [2008] have summarized several years of paleoseismological studies throughout the Apennines and concluded that the studied fault system might have ruptured once at 2–3 ka. Therefore, most authors point to an event occurring on the Rotella-Aremogna fault system at less than 3–4 ka.

3. Sampling, ^{36}Cl, and Chemical Analysis

To recover the Holocene seismic history of the Pizzalto fault, the ^{36}Cl cosmic ray exposure dating technique has been used. Already applied to other normal faults in the Mediterranean area, this method has proven to be

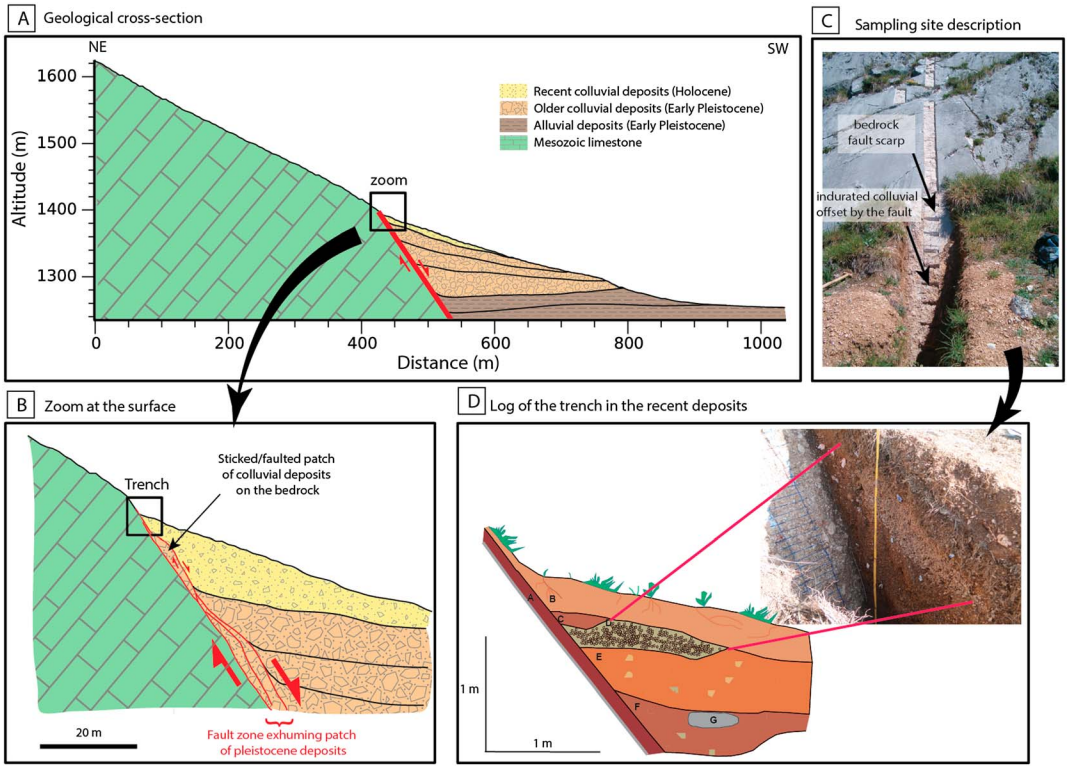

Figure 3. Deposit analysis: (a) Geological cross-section perpendicular to the Pizzalto fault. (b) Zoomed in cross section showing fault zone with partially dragged and faulted colluvial deposits. (c) A 4.4 m of sampled exhumed fault plane, with a ~2 m deep open trench at the bottom of the scarp. (d) Trench log: A—faulted colluvial sediments with sparse subangular limestone pebbles 2 to 8 cm in size. B—greyish brown soil. C—brown paleosol (no pebbles). D—medium gravel with coarse to very coarse pebbles in yellowish brown silty matrix. E—fine gravel in brown-grey sandy matrix. F—similar to unit E but with more abundant and coarser matrix. G—decametric limestone pebble.

efficient to recover the slip and age of past exhumational events on limestone bedrock fault planes [*Mitchell et al.*, 2001; *Benedetti et al.*, 2002, 2003; *Schlagenhauf et al.*, 2010, 2011; *Palumbo et al.*, 2004; *Benedetti et al.*, 2013; *Benedetti and van der Woerd*, 2014]. It is based on the accumulation of in situ-produced ^{36}Cl in limestone rocks exposed to cosmic rays. When a part of the fault plane is buried, it is protected from interaction with cosmic rays; when it becomes exhumed, ^{36}Cl starts to accumulate in the exposed limestone rocks.

The sampling site is located at the southern tip of the fault, where the fault scarp is the highest, to recover the maximum slip per event (Figure 2). The site is located away from rivers or gullies to avoid erosion and scarp exhumation by river incision or colluvial collapse and to ensure that the lower surface has been preserved. It is assumed that no significant erosion has affected the scarp, the surface below the scarp, or the surface above the scarp. The scarp is approximately 10 m high and dips 56°SW. The lowest 4.5 m corresponding to the best preserved striated part of the scarp was sampled (see all site parameters in Table S2). There was no apparent recent debris at the base of the scarp, which is covered by approximately 50 cm of soil.

Sampling consists of peeling off the scarp, from the top to base. To have a continuous record along the scarp and to avoid a fractured and altered part, a portion of the sampling was laterally shifted by 20 cm (Figure 3c). Thereby, 4.4 m of the exhumed scarp was continuously sampled, generating 44 slabs of rocks, each of which were 3 cm thick, 15 cm wide, and 10 cm long. Moreover, a ~2.5 m deep trench was dug in the colluvial deposit at the base of the scarp to sample the buried part of the fault plane. Ten samples were taken to a maximum depth of 2.25 m.

In the trench, a portion of the fault plane was covered by an approximately 5–10 cm thick layer of cemented colluvial breccia, suggesting that the cemented breccia might also have been faulted (Figure 3b). The stratigraphy exposed in the trench includes paleosols and coarse colluvial deposits gently dipping southwestward (Figure 3d).

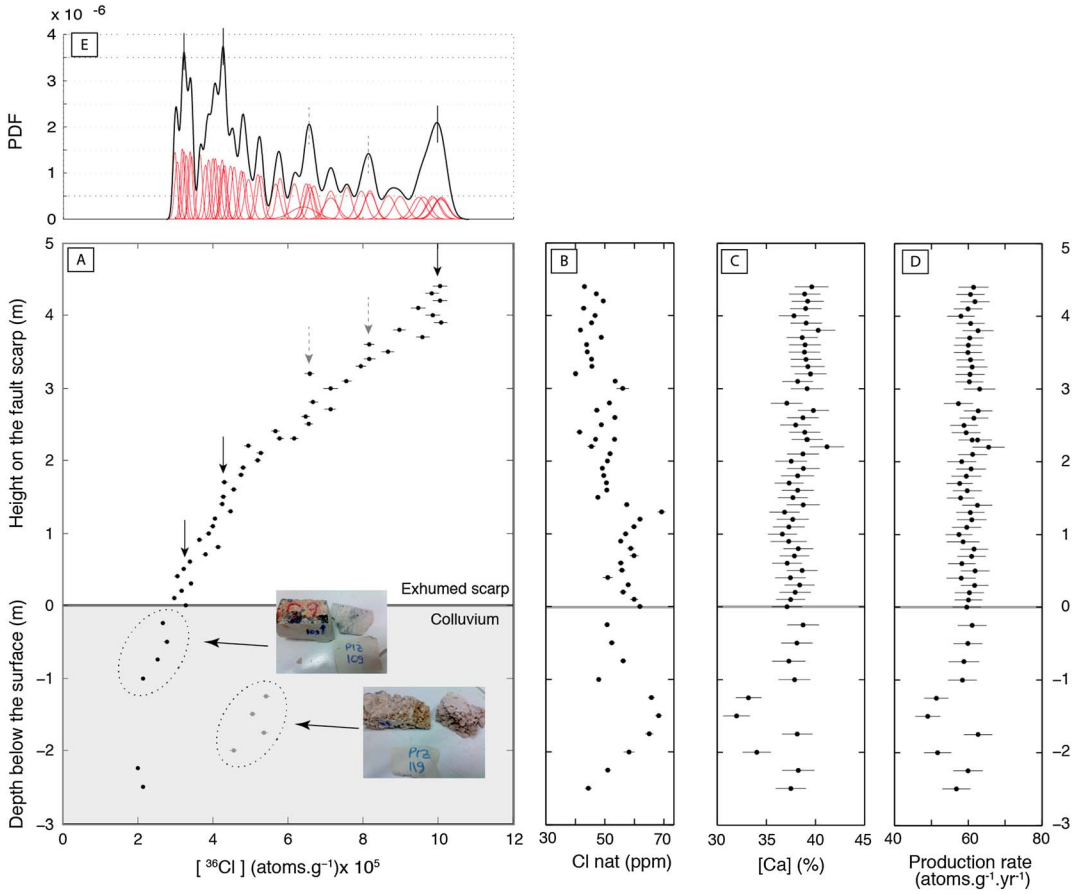

Figure 4. (a) [^{36}Cl] AMS measurements as a function of the scarp height. Horizontal lines correspond to 2σ AMS uncertainties. Vertical black arrows indicate major discontinuities identified in the [^{36}Cl] data. Dashed grey arrows suggest more subtle discontinuities. Grey dots show samples from cemented breccias, with pictures of samples from the fault scarp and from the cemented breccias. (b) Natural chlorine concentration as a function of scarp height. (c) Calcium concentration as a function of scarp height. (d) ^{36}Cl production rate of each sample calculated from their individual chemical composition. (e) Individual probability density functions (PDFs) (red) and summed PDFs (black). Three major peaks (dark vertical lines) and two more subtle peaks (dashed vertical lines) are outlined. These peaks are not related to the chlorine or calcium contents.

The density of the colluvial wedge material has been estimated to be ~1.7 g cm^{-3} by weighing the material in a box of known volume (Table S2).

The samples were crushed, sieved, and chlorine was chemically extracted using AgCl. Natural Cl (hereafter Cl_{nat}) and ^{36}Cl were then determined via isotope dilution accelerator mass spectrometry based on the measured ^{35}Cl/^{37}Cl and ^{36}Cl/^{35}Cl ratio measurements performed at the French national accelerator mass spectrometry (AMS) facility Accélérateur pour les Sciences de la Terre, Environnement, Risques (ASTER) (CEREGE, Aix-en-Provence, France). The ^{36}Cl and Cl concentrations were normalized to a ^{36}Cl standard prepared by K. Nishiizumi: KNSTD1600, with a nominal ^{36}Cl/^{35}Cl value of $2.11 \pm 0.06 \times 10^{-12}$ [*Sharma et al.*, 1990; *Fifield et al.*, 1990]. The decay constant of $2.303 \pm 0.016 \times 10^{-6}$ yr^{-1} used corresponds to a ^{36}Cl half-life ($T_{1/2}$) of 3.014×10^5 years. The analytical uncertainties include counting statistics, machine stability, and blank correction. The measured ^{36}Cl concentrations range from ~10^6 to ~10^7 atoms, 400 times higher than that measured in the blanks (10^4 atoms of ^{36}Cl). The Cl concentrations in the samples range from ~2.10^{19} to ~4.10^{19} atoms, whereas blanks contain less than 10^{16} atoms of Cl (Table S3).

The natural Chlorine concentrations are on average 50 ppm, with some samples reaching up to 70 ppm (Figure 4b). The different pathways of ^{36}Cl are as follows: spallation of target elements (78%), thermal and epithermal neutron capture (15%), and slow negative muons capture (7%) [*Schimmelpfennig et al.*, 2011]. It is interesting to note that the samples from the lower portion of the fault scarp (between the base and

140 cm high) have Cl concentration that are 15% higher (58 ppm on average) than the average of all the other samples (48 ppm on average) (the uncertainty associated with the Cl concentration is approximately 1 ppm, Table S3 and Figure 4b). Careful examination of the samples and of the lower portion of the fault scarp does not reveal any significant difference in the geology or in the visual appearance of the lower portion, including no alteration, vegetation, or fissures. There is no correlation with the Ca content, which is common across all the samples. It is possible that among the carbonate layers, one layer may have incorporated more Cl during diagenesis, resulting in slightly different Cl concentrations.

Four of the samples collected within the colluvium are evident outliers in the ^{36}Cl concentration depth profile (Table S3 and Figure 4a). The natural chlorine (Cl_{nat}) concentration of these four samples is high, with values between 58 and 68 ppm (Table S3 and Figure 4b). The Ca concentration of three of these samples is also significantly lower than that of all other analyzed samples (Table S3 and Figure 4c). Those three samples are lithologically different because they are cemented colluvial deposits (see picture Figure 4a); thus, they are composed of different clasts cemented within a partly altered carbonate matrix.

Next, we discuss how the chemical composition might interfere with the ^{36}Cl data interpretation in terms of exhumational events.

4. ^{36}Cl Data Interpretation

The samples exposed on the fault scarp originally emerged from below the colluvium and were exposed at the surface by slip events. The evolution of the ^{36}Cl concentration along a depth profile while the fault section is buried under the colluvium exhibits a depth-dependent exponential relationship [e.g., *Gosse and Phillips*, 2001]. Therefore, prior to full exhumation, the ^{36}Cl concentrations that have been accumulated below the surface exhibit an exponential evolution reflecting the scarp preexposure history. Once a portion of the scarp is exhumed, which is assumed to be the result of a large earthquake, ^{36}Cl continues to accumulate but at a constant rate, regardless of location along the exposed scarp. Therefore, the ^{36}Cl concentration ([^{36}Cl]) of an exhumed sample is the sum of the ^{36}Cl produced while it was buried under the colluvium prior to the earthquake (preexposure history) and of the ^{36}Cl accumulated when it was exposed at the surface after its exhumation by the earthquake. For normal fault scarps resulting from a succession of earthquakes, the [^{36}Cl] profile along the fault plane height is theoretically a series of exponential curves separated by discontinuities [*Schlagenhauf et al*., 2010]. Identification of those discontinuities in the [^{36}Cl] profile allows estimating the number of large past earthquakes that affected the fault plane at the surface and quantifying their associated slips. Modeling the [^{36}Cl] profile over its entire length will then provide the ages of these major events. *Schlagenhauf et al*. [2010] suggest from theoretical calculations and their comparisons with [^{36}Cl] measured profiles that small events with slip lengths of less than 25 cm and earthquake ages that differ by less than a few 100 years cannot be resolved. These limitations imply that the number of earthquakes determined using the ^{36}Cl approach is always a minimum because some events may actually represent several small temporally close events [cf. *Schlagenhauf et al*., 2010; *Benedetti et al*., 2013].

Production rate variations (Figure 4d) linked to variable Ca and Cl contents are most likely responsible for the measured ^{36}Cl concentrations not increasing regularly with the scarp height. This variability is accounted for while modeling the data. To bring out the major discontinuities along the [^{36}Cl] profile, the probability density functions (PDF) of the sample concentrations are analyzed [*Lowell*, 1995; *Schlagenhauf et al*., 2010]. The PDF of a sample is a Gaussian curve whose 2σ width corresponds to its analytical uncertainty. Summing individual PDFs along the profile reveals clusters of points with nonsignificantly different concentrations. Along the [^{36}Cl] profile, the resulting peaks reveal the almost constant [^{36}Cl] observed in the deeper parts of the [^{36}Cl] exponential profile with depth that characterizes the [^{36}Cl] concentration evolution along the paleoburied scarp.

^{36}Cl concentrations vary from the top to the bottom of the exhumed profile between 1×10^6 to 3×10^5 atoms/g rock. Visual identification and summed PDFs (Figure 4e) reveal three major discontinuities at 2.9–3.1, 4.1, and 10.0×10^5 atoms of ^{36}Cl per gram of rock. The discontinuity at 4.1×10^5 atoms of ^{36}Cl/g of rock (sample at 130–150 cm) might appear correlated with the shift in Cl concentration; however, this discontinuity involves five points with similar ^{36}Cl concentration but variable Cl concentrations (from 45 to 60 ppm). Two more subtle peaks are suggested at 6.4 and 8.1×10^5 atoms of ^{36}Cl/g of rock. They are less constrained because of the relatively large

uncertainty associated with the AMS measurement of the sample at 2.9 m and the very few samples contributing to the peak (only 2 for the peak at 8.1×10^5 atoms of ^{36}Cl/g of rock). Hence, this set of data thus suggests that 3 to 5 slip events must have been necessary to shape the [^{36}Cl] profile.

The samples collected from the fault scarp within the colluvium have ^{36}Cl concentrations that vary between 2 and 3×10^5 atoms of ^{36}Cl/g of rock. The upper sample concentrations decrease with depth as expected, whereas deeper samples made of indurated colluvial material have ^{36}Cl concentrations that are significantly higher than those expected from an exponential decrease. It is possible that fluid recrystallization during cementation of the colluvial material has affected the ^{36}Cl content of these samples or that the pebbles incorporated in the colluvial material have been previously exposed. The ^{36}Cl contained in these samples thus appears enhanced by an additional inherited ^{36}Cl component. To avoid generating high discrepancies while modeling the data, these samples are considered as outliers and are not included in the modeled data set.

5. Trace Element Analysis

To complement the ^{36}Cl cosmogenic nuclide analysis of the samples, the major and trace elements in each sample were measured to explore whether concentration changes in trace elements along the fault scarp might be used as another tracer of exhumational events. This method was first described and developed by *Carcaillet et al*. [2008] and *Manighetti et al*. [2010] for the Magnola fault (central Apennines, Italy).

Because calcite bulk equilibrium is weak, many environmental factors lead to its degradation or dissolution, particularly in acidic conditions [*Sweeting*, 1966; *Trudgill*, 1985; *Smith et al*., 2000; *Plan*, 2005]. Such conditions are favored by rainfall, CO_2-rich fluid circulation, roots and microbial respiration, and organic material oxidation, and they occur particularly in the upper 30–50 cm of the soil [*Reardon et al*., 1979; *Paul and Clark*, 1989; *Fierer et al*., 2003]. On a normal fault such as the Pizzalto fault, the limestone footwall is directly in contact with the colluvium soil. The limestone rock might thus undergo chemical reactions and modifications (mainly dissolution and recrystallization) at this contact. Trace elements such as REE-Y (rare earth elements and yttrium) are highly concentrated in soil [*Duddy*, 1980; *Dia et al*., 2000; *Taunton et al*., 2000; *Tyler*, 2004; *Song et al*., 2006; *Pourret et al*., 2007]. Acidic conditions at the contact with soil might trigger some recrystallization of the surface of the buried footwall, which might then incorporate REE-Y along the grain boundaries [*Carcaillet et al*., 2008]. *Carcaillet et al*. [2008] and *Manighetti et al*. [2010] have associated peaks in REE-Y concentrations, measured in samples collected along the footwall, to exhumational events, with the peak marking the topmost part of the exhumed portion of the fault plane.

Major and trace element contents along the fault plane were measured in the two first centimeters of each rock slab, corresponding to the fault plane surface. Chemical preparation and measurements were performed at Service d'Analyse des Roches et des Minéraux (SARM) (CRPG, Nancy, France), using ICP-MS X7 (Thermo Scientific) and ICP OES Icap 6500 (Thermo Scientific) for major and trace elements, respectively. The extended protocol is available on *Carignan et al*. [2001]. Uncertainties range from 5% to 15%. The major and trace element contents are available in Tables S4 and S5.

The vertical evolution of the concentration of each major and trace element, including REEs and yttrium (Y), can be found in Figure S6. The REE-Y concentration corresponds to the concentration of each element (Ci) normalized by the mean concentration of the elements along the scarp height (Cm). The REE-Y concentrations plotted against the scarp height exhibit a similar background value above which some samples display significantly higher values (see in Figure S7). To quantify the amplitude Δi between the background value and the higher values, we calculated the difference between Ci, the concentration of an element in a sample, and Cm, the mean concentration of this element along the scarp height. We then normalized each peak amplitude by Δm, the mean absolute value of those differences ($\Delta m = \sum |\Delta i| / N$, where N is the number of samples). The results are shown in Figure 5a. For each sample, we also calculated the mean amplitude value (red dot) of all the analyzed elements (REE-Y) and the standard deviation. Overall, the standard deviations are small (0.3 on average) in the exhumed part and higher in the buried part (1 on average).

The ΔREE-Y concentrations have a similar trend along the fault scarp height, with portions of linearly decreasing concentrations interrupted by sharp and abrupt increases. The differences between the enhanced concentrations and the concentrations along the linear portions range from 1.0 to 1.5. This trend

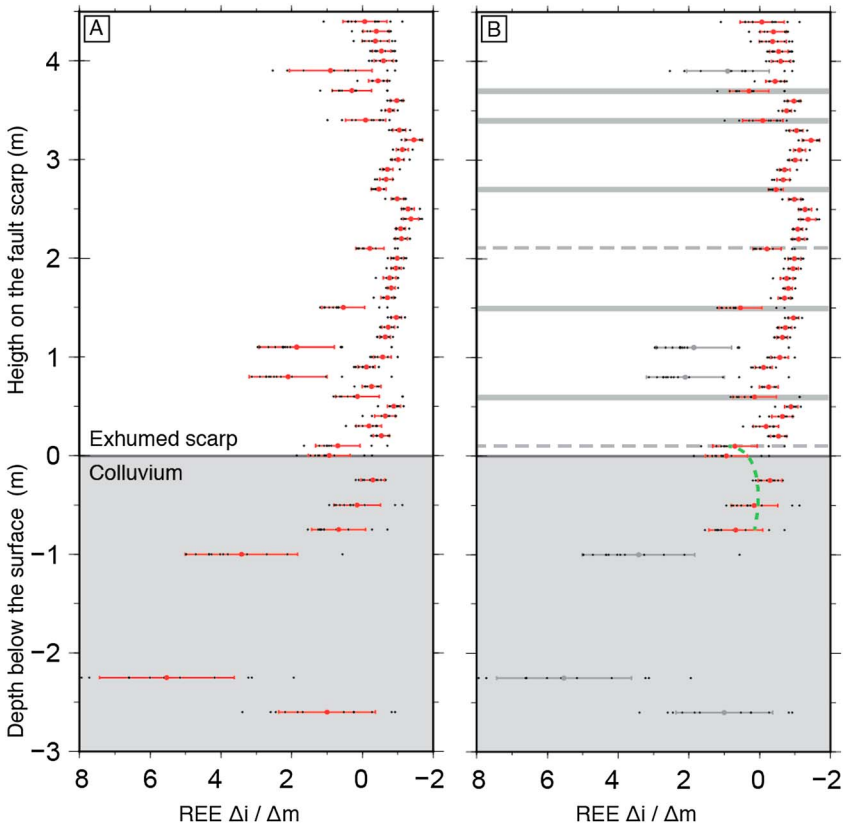

Figure 5. (a) Evolution of REE-Y concentrations along the scarp. For element (i), the *X* axis to the measured peak amplitude, Δ*i*, which is the difference between the element (i) concentration in the sample (Ci) and its average concentration for the whole scarp (Cm) normalized to the averaged peak amplitudes for the whole scarp (Δ*m*). Horizontally aligned black dots represent Δi/Δm for all measured elements. The red dot represents the Δ*i*/Δ*m* average of all elements within a sample, and horizontal red lines represent their associated standard deviations. (b) Identification of peaks in the REE-Y data.

is also observed along the buried part of the scarp, not considering the three lowest data points measured in samples composed of indurated colluvial material. Additionally, unlike what is expected, the highest concentration near the interface between the exhumed and buried parts is present in the sample collected 10 cm above the base of the scarp. This could be due to a slight packing of the soil after the most recent earthquake, which induced a small exhumation (≤10 cm) of the fault scarp. This process might occur at any time, thus increasing the uncertainty on the slip per event by approximately 10 cm. However, it should not affect the age results.

Carcaillet et al. [2008] and *Manighetti et al.* [2010] observed similar peaks and interpreted them as being transitional zones between the exhumed and the buried parts of the scarp. However, they did not notice linear decreases punctuated by abrupt peaks but rather constant concentrations separated by pulses of increased concentrations. The differences between the constant concentrations and the peak concentrations they observed are on the same order as those measured at Pizzalto. The overall REE-Y concentrations measured at Pizzalto are on average 63% lower than those measured at the Magnola site by *Carcaillet et al.* [2008] and *Manighetti et al.* [2010].

We interpret the repeated pattern along the Pizzalto profile as representing different portions of the scarp that have been successively exposed to soil-forming conditions. The shift between an almost linear depletion in REE-Y and an abrupt increase in REE-Y concentrations marks the transition between buried and exposed sections of fault plane. Moreover, only peaks associated with a standard deviation of less than 1 (increased concentrations supported by all REE-Y) are considered (peaks at 0.8, 1.1, and 3.9 m are ignored) (see Figure 5b). Using this approach, six discontinuities are clearly identified at 0.0, 0.6, 1.5, 2.7, 3.4, 3.7 m (grey lines), and a less defined additional one at 2.1 m (grey dashed lines).

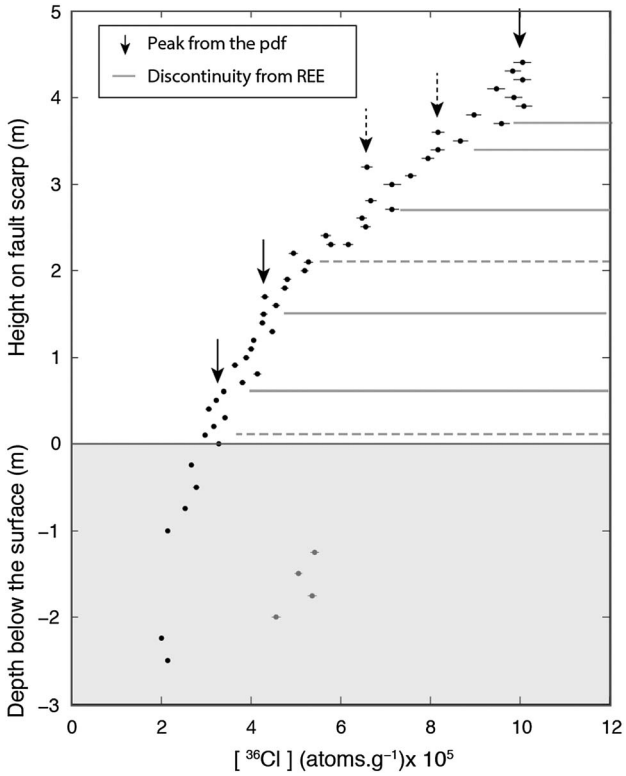

Figure 6. [^{36}Cl] as a function of scarp height. Black continuous/dashed vertical arrows indicate major/minor discontinuities in [^{36}Cl] sample measurements revealed by the PDFs and visual inspection. Grey buried dots represent four abnormally enriched cemented breccia samples. Vertical grey lines outline peaks in the REE-Y data. Dashed grey lines indicate minor peaks.

6. Exhumation History of the Pizzalto Fault

6.1. Comparison Between [^{36}Cl] and [REE-Y] Data

Recovering the exhumation history of the Pizzalto fault involves determining the number and the amplitude of slip events. We integrate and compare the two data sets described above, [^{36}Cl] and [REE-Y] (Figure 6). The discontinuities in the [^{36}Cl] profiles detected through stacked PDFs are outlined by vertical arrows, and the [REE-Y] peaks are marked by horizontal grey bars. Both data sets are associated with a shift from previously buried parts to exhumed parts. From the top to the base, we observe (1) the first PDF peak at 3.6–3.8 m corresponds to a [REE-Y] peak at 3.7 m; (2) a small PDF peak involving only 2 points suggests a discontinuity at approximately 3.4–3.3 m and is supported by a peak in [REE-Y] at 3.4 m; (3) another small PDF peak associated with 4 points located between 2.9 and 2.5 m matches a [REE-Y] peak at 2.7 m; (4) a well-defined PDF peak between 1.4 to 1.7 m matches the [REE-Y] peak at 1.5 m; and (5) another well-defined PDF peak at 0.5–0.6 m matches a [REE-Y] peak at 0.6 m. Finally, the base of the scarp is also associated with a [REE-Y] peak at 0.1 m. The less prominent [REE-Y] peak at 2.1 m does not seem to be associated with any prominent peak in the PDF.

In summary, the five most prominent peaks detected using stacked PDFs of the ^{36}Cl concentration data correspond to the five peaks detected in the REE-Y concentration data. Considering the intervals corresponding to the scarp sections, this pattern suggests that six slip events have contributed to the exhumation of the Pizzalto fault scarp and to shape the ^{36}Cl concentration profile.

6.2. A Monte Carlo Approach to Constrain the Exhumation History

To better constrain this proposed scenario of six exhumation events, the various exponential sections shaping the [^{36}Cl] profile associated with different exhumation events have been modeled using a Monte Carlo-based inverse approach. For this purpose, we used the code provided by *Schlagenhauf et al.* [2010], which calculates, from a determined scenario, the theoretical [^{36}Cl] profile that should be observed today. The necessary input parameters of this code are the age of each event, the associated slip, and the preexposure value to account for the exposure history of rocks prior to the older event actually detected. The likelihood of an exhumation scenario is then assessed through three criteria based on the comparison of the theoretically determined [^{36}Cl] to the measured [^{36}Cl]: (i) the weighted root-mean-square (RMSw) quantifies the goodness of fit between measured and theoretical [^{36}Cl], taking into account the measurements uncertainties; (ii) the Akaike information criterion (AICc) [*Akaike*, 1974; *Burnham and Anderson*, 2002] introduces the number of free parameters in the calculation, favoring the simplest models; and (iii) the chi-square (χ^2) takes into account both uncertainties in the measurements and the number of free parameters. The more realistic scenarios are those leading to the lowest RMSw, χ^2, and AICc values. The optimization is an iterative process that consists of successively determining the preexposure and event ages going from oldest to youngest, the latter being affected by the older events.

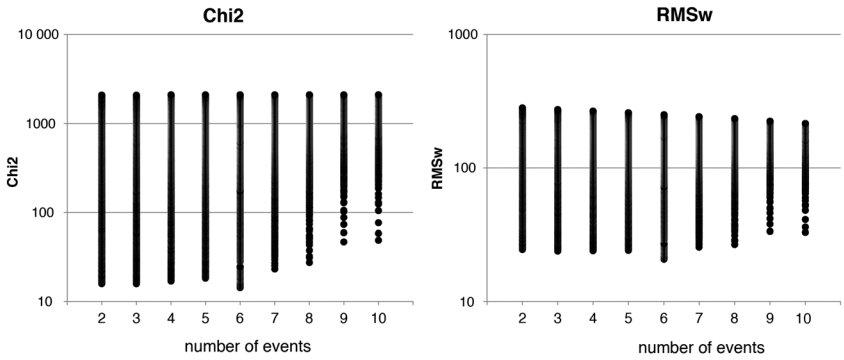

# itereations	# events	Slip per event (cm)	Ages (yr)	min RMSw	min Chi2
36000 (4000 x 9)	2 - 10	10 -360	500 -10 000	29.1	23.6

Figure 7. Results from a Monte Carlo analysis showing RMSw and χ^2 results from 36,000 randomly tested scenarios. The best profiles, i.e., those associated with the lowest χ^2 and RMSw values, were obtained using six events. The misfit function clearly increases for scenarios using more than six events.

Input model parameters related to the site geometry, rock/colluvium density, and scaling factors (shielding) are presented in Table S2. The chemical composition of the fault scarp and of the colluvial wedge samples can be found in Tables S3–S5. The geometry of the fault is used to calculate the shielding factors involved in the modeling. It can simply be described through (i) α, the dip of the colluvium surface; (ii) β, the dip of the fault scarplet plane at the surface; (iii) γ, the dip of the older eroded fault section above the scarplet; and (iv) H, the height of the postglacial scarp. The ^{36}Cl production rate from spallation of calcium has been calibrated in Sicily by *Schimmelpfennig et al.* [2011]. Because the Pizzalto fault is located almost at the same latitude and elevation as this calibration site and because the exposure duration of both sites is similar, we used the calibrated production rate of 42.2 ± 4.8 atoms of ^{36}Cl/g of Ca/yr. *Schlagenhauf et al.* [2010] demonstrated that the variability in the geomagnetic field intensity at the latitude of the study and over the time period investigated (the Holocene) is negligible. Scaling with respect to latitude and elevation was therefore performed considering constant geomagnetic field intensity and using the *Stone* [2000] scheme. The erosion rate of the fault scarp is also parameterized in the model, but because the scarplet surface is well preserved with slickensides, we choose to neglect it.

To be able to explore a wide range of possible scenarios (number of exhumations, ages of occurrence, and slip per event), a classical Monte Carlo approach was developed. The goodness of fit of 4000 models per each possible scenario (2 to 10 events) has been evaluated, and the preexposure, number of events, slip per event, and slip ages were assigned random values within defined ranges (see the table in Figure 7). The results of these analyses are shown in Figure 7 and suggest that (1) if the number of exhumation events is greater than 7, the goodness of fit leads to higher (thus worse) values relative to a lower number of exhumation events and (2) among the 36,000 tested scenarios, the scenario that best reproduces the [^{36}Cl] profile, both in terms of RMSw (29.2) and χ^2 (23.6), is that involving six events at 3.2 ka (slip per event: 0.5 m), 3.2 ka (slip per event: 0.4 m), 2.1 ka (slip per event: 0.4 m), 1.3 ka (slip per event: 1.1 m), 1.1 ka (slip per event: 0.9 m), 1.0 ka (slip per event: 1.1 m), and a preexposure of 16.1 kyr. Figure 8a represents the ^{36}Cl concentration versus the height of the scarp derived from this scenario. The number of events determined using this approach is similar to that derived from the analyses of the [^{36}Cl] and [REE-Y] signals in sections 3 and 4. The position along the scarp height of the discontinuities derived from the [^{36}Cl] + [REE-Y] signal analyses, and the modeling of the [^{36}Cl] differs slightly (Figures 6 and 8a), and the difference in slip per event is at most 40 cm, with a mean of 20 cm.

6.3. The Most Realistic Exhumation Scenario

Using the slip derived from the [^{36}Cl] + [REE-Y] analyses (Figure 6) and the modeling (Figure 8a), the most realistic exhumation scenario and the associated uncertainties are now explored.

Following the procedure of uncertainty determination defined by *Schlagenhauf et al.* [2010], we estimate the epistemic uncertainties (e.g., uncertainties due to the current lack of knowledge that cannot be reduced by a

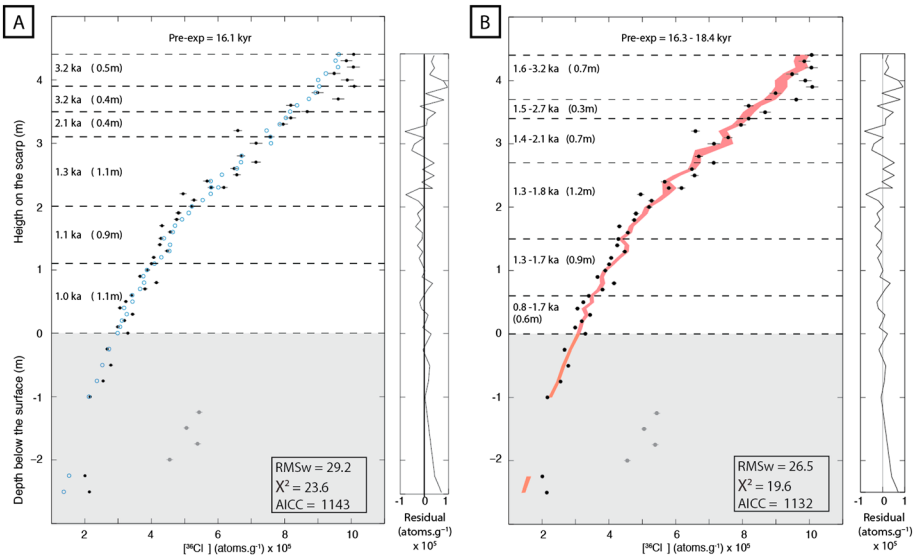

Figure 8. (a) Modeling of the [^{36}Cl] data along the Pizzalto fault scarp using the optimum scenario determined via the Monte Carlo approach. Theoretical (blue dots) and measured (dark dots with 2σ AMS uncertainties) [^{36}Cl] profiles are shown as a function of the Pizzalto fault plane height. Dashed dark lines indicate portions of the scarp exhumed during each slip event. The residuals are the differences between the measured and theoretical [^{36}Cl] data. Grey buried dots are four abnormally enriched cemented breccia samples. (b) Modeling data using slip magnitudes derived from [^{36}Cl] + [REE-Y] analyses and integrating the analytical uncertainties. The red shading represents all possible models fitting the data.

probabilistic approach) to be 1–5%. They include site geometry (dip of colluvium and scarp), measurements of chemical elements, and rock and colluvium densities. Uncertainty on the ^{36}Cl production rate was determined to be 5–10% by *Schimmelpfennig et al*. [2011]. Those are uncertainties independent from the tested models that apply equally to all ages.

To estimate the uncertainties on the determined ages, the analytical uncertainty associated with the [^{36}Cl] measurements has been propagated in our best scenario. For this purpose, AMS-measured [^{36}Cl] standard deviation values of the samples are added to the best theoretical [^{36}Cl] profile, defining a 1 sigma uncertainty envelope (Figure 8b). All event ages leading to a model that fits within this envelope are then considered. Their range, as well as the range of the associated slips, defines the uncertainty on the age and on the slip. The maximum uncertainties are ±1.3 kyr on ages and ±30–50 cm on displacements.

The last source of uncertainty is the preexposure age, which integrates the history of exhumation and exposure prior to the oldest determined earthquake. This uncertainty is difficult to estimate because it mostly depends on the fit between the model and the data in the upper part of the [^{36}Cl] profile. The preexposure value, however, mainly impacts the age of the first (oldest) event and only slightly impacts the younger ones [*Schlagenhauf et al*., 2010; *Benedetti et al*., 2013]. Moreover, there is no evidence of long-term fault activity, such as triangular facets or wine glass valleys. This suggests that no significant motion has occurred on the fault prior to the onset of the bedrock fault scarp exhumation; therefore, a long time period preceded the first fault exposure, in agreement with a long preexposure duration (≥15 ka).

Figure 8b shows the modeled [^{36}Cl] profile (in red) as a function of the scarp height, obtained from the best scenario (lowest RMSw and χ^2 values of 26.5 and 19.6, respectively) involving six events (called S6). The six events occurred at 3.2–1.6 ka (slip per event: 0.7 m), 2.7–1.5 ka (slip per event: 0.3 m), 2.1–1.4 ka (slip per event: 0.7 m), 1.8–1.3 ka (slip per event: 1.2 m), 1.7–1.3 ka (slip per event: 0.9 m), and 1.7–0.8 ka (slip per event: 0.6 m), with a preexposure duration of 16–18 kyr. Comparing the theoretical [^{36}Cl] profile to the data (dark dots), a smooth curve that closely follows the trend of the data is observed. The variability in the data, particularly at 3.7–4.0 m, 2.3–2.6 m and at 0.6–0.7 m, is smoothed in the model, suggesting that those discrepancies are not due to the specific chemical composition of the samples but to other undetermined processes. The residual (measured [^{36}Cl]-theoretical [^{36}Cl]) is lower for the lowest (thus younger) part of the scarp, from 0.0 m to 2.0 m, than for the upper (older) part. Along the buried scarp, the theoretical [^{36}Cl] data fit the measurements to a depth of 1 m, as well as the results for the two deepest samples.

If we assume that the four altered indurated colluvial samples have been affected by a nonnegligible proportion of ^{36}Cl produced prior to deposition (for example, when the pebbles where screen on top of the scarp), the difference between the [^{36}Cl] of the theoretical profile and the current concentration is ~3.10^5 atoms of ^{36}Cl per gram of rock, which would correspond to 5 kyr of exposure prior to their deposition. The two deepest samples are also colluvial breccia and might therefore have been affected by inheritance. Similarly, the discrepancy between the model and the ^{36}Cl measured concentrations of ~5.10^4 atoms of ^{36}Cl per gram of rock corresponds to 0.8 kyr of exposure prior to their deposition.

In summary, the upper part of the buried scarp is satisfactorily modeled by the selected exhumation history, while the samples collected in the lower part, belonging to different lithological units, have probably experienced inheritance which could explain the discrepancies between the model and the data.

Finally, outside the range of possible scenarios, we tested two extreme cases: (i) a single-event scenario that exhumed the whole 4.4 m height of the scarp and (ii) a 22-event scenario (S22) that exhumed the scarp progressively, with each slip being 0.2 m, thus mimicking creeping. The best solution for S1 requires an event at 1.6 ka and a preexposure duration of 18 kyr (RMSw = 26.5), whereas the best solution for S22 requires a succession of events between 3.0 and 1.0 ka and a preexposure duration of 16 kyr (RMSw = 28.6) is required (Figure 9).

The similarity of the RMSw values associated with the S6 and S1 scenarios suggest that they both reproduce the ^{36}Cl profile, whereas the RMSw value for the S22 scenario is slightly higher (28.6) and, above all, does not fit the upper part of the profile. When comparing the range of ages obtained in each scenario (S1: 1.6 ka, S6: 3.2 to 0.8 ka, and S22: 3.0 to 1.0 ka), we observe that although the number of events is different, all models suggest that the scarp was exhumed within a similar time period, i.e., between 3.2 and 1.0 ka, with active exhumation lasting at most 2.4 kyr. All scenarios suggest similar preexposure durations (~16–18 kyr), and the larger the number of events, the lower the preexposure duration (S1: 16 kyr, S6: 16–18 kyr, and S22: 18 kyr). All models suggest that no major events have exhumed the Pizzalto fault scarp for 0.8–1.6 kyr.

The modeling thus implies that the Pizzalto fault scarp is younger than 3.2 kyr and has been exhumed by a succession of events, which we interpret as being surface-rupturing earthquakes, between 3.2 and 0.8 ka.

7. Discussion

7.1. Earthquake Event Ages, Slip, and Magnitude Based on the ^{36}Cl and REE-Y Data Set

The analysis of the [^{36}Cl] and [REE-Y] data and the modeling of the [^{36}Cl] of the first 4.4 m of the 10 m high Pizzalto fault scarp suggest that this portion was exhumed over a time span lasting less than 2.4 kyr. The best scenario suggests six large events with slip per event between 0.3 m and 1.2 m. A scenario with a 4.4 m high single event also explains the ^{36}Cl data. This single-event scenario, however, does not account for the presence of the REE-Y discontinuities, whereas the scenario with six events integrates both the ^{36}Cl and REE-Y data sets. Our analysis thus shows that for the conditions prevailing at the study site, the REE data provide additional constraints and allow for the determination of the most likely slip history.

Dispersed [^{36}Cl] measurements result in poorly expressed exponential discontinuities that make identifying the number of events and their associated slips difficult. Short interseismic periods and moderate slips ($<$1 m) can produce "smooth [^{36}Cl] profiles" because the time interval between two successive events is not long enough to generate a fully developed exponential decrease in [^{36}Cl] as a function of depth in the buried part. In all scenarios, a long preexposure duration implies that a significant amount of the measured [^{36}Cl] has been accumulated in the buried footwall prior to scarp exhumation, with the predominant production pathway at depth below 1.5 m being through nuclear reactions induced by negative muons [*Schimmelpfennig et al*., 2009; *Braucher et al*., 2003]. The amount of ^{36}Cl produced at depth during such a long preexposure duration is therefore nonnegligible. We estimated that the amount of ^{36}Cl that has accumulated since the various scarp sections have been exposed at the surface ranges from 1.0 to 8.9×10^5 atoms of ^{36}Cl per gram of rock, i.e., approximately 75 to 90% of the total measured concentrations.

However, [REE-Y] exhibits a common and repeatable pattern along the scarp that we associated with the exhumation events and that are well correlated with the [^{36}Cl] discontinuities. *Carcaillet et al*. [2008] and *Manighetti et al*. [2010] have observed similar patterns, and their [REE-Y] peaks are also correlated with the

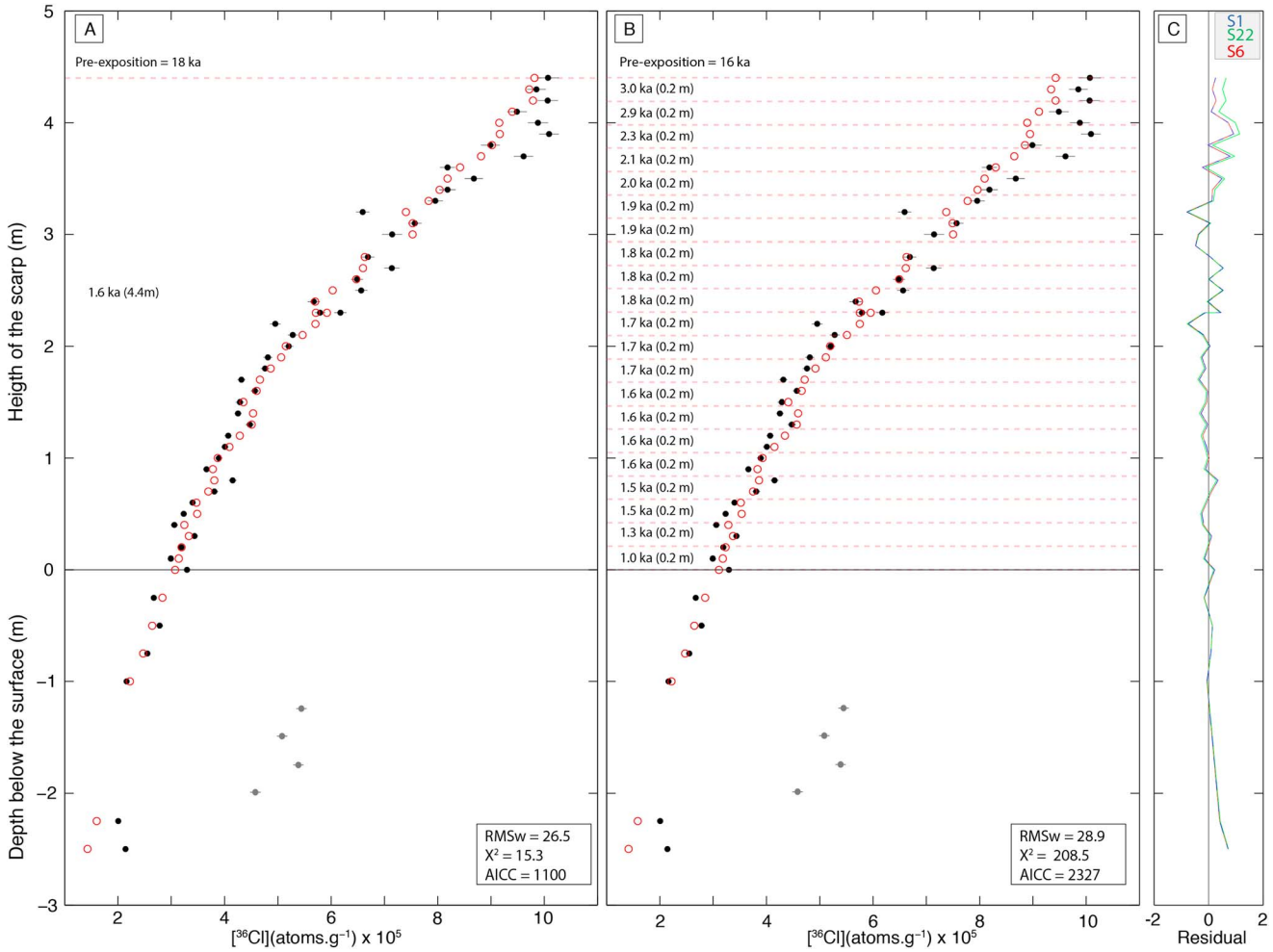

Figure 9. Modeling [^{36}Cl] data using two extreme scenarios: (a) a single 4.4 m event (called S1) and (b) 22 events with 0.2 m of slip per event (called S22). Theoretical (red dots) and measured (dark dots) [^{36}Cl] are plotted as a function of the Pizzalto fault plane height. Horizontal red lines indicate portions of the scarp exhumed during each slip event. (c) The residuals correspond to the differences between the measured and theoretical [^{36}Cl] data for S1, S22, and S6 (see Figure 8b). Note that the S1 and S6 residuals are almost identical.

[^{36}Cl] discontinuities. The pattern observed at the Pizzalto fault differs from that observed at the Magnola fault [*Carcaillet et al*., 2008; *Manighetti et al*., 2010]. Although the portion of the scarp exposed to soil exhibits an abrupt increase in the REE-Y concentration, the REE-Y concentration in the deeper part of the buried section tends to increase at the Pizzalto fault but decrease at the Magnola fault. The difference in the [REE-Y] pattern between the Magnola fault and the Pizzalto fault might be linked to the nature of the colluvium, which differs from one fault to another. At Pizzalto, the soil thickness is less than at Magnola, and there is no indurated colluvium in the bottom part at Magnola. This might control the spatial distribution of REE-Y contents in the colluvium and, thus, the enrichment of the fault scarp. The processes associated with REE-Y accumulation in the colluvium and exchange with the fault bedrock remain unclear. Reactions within the soil enhance the enrichment of the fault plane [*Moraetis et al*., 2015; *Carcaillet et al*., 2008]. Soil thickness, as well as climatic parameters (elevation and amount of precipitation), might influence its composition and thus the exchange with the bedrock. Additional studies on those aspects are necessary to improve our understanding of the processes underlying the exchanges of REE-Y between soil and bedrock fault planes. In the future, the chemical composition of the soil should be assessed to be able to compare results between sites.

In summary, the scenario that best reproduced both the [REE-Y] and the [^{36}Cl] discontinuities involves six events at 3.2–1.6 ka (slip per event: 0.7 m), 2.7–1.5 ka (slip per event: 0.3 m), 2.1–1.4 ka (slip per event: 0.7 m), 1.8–1.3 ka (slip per event: 1.2 m), 1.7–1.3 ka (slip per event: 0.9 m), and 1.7–0.8 ka (slip per event: 0.6 m), and a preexposure duration of 18–16 kyr. Three groups of events emerge from this model: (1) the

youngest event might have occurred between 0.8 ka and 1.7 ka, (2) two events with ages between 1.3 and 1.8 ka are not significantly different, and (3) three older events with smaller slip per event values and ages in the range of 1.4 to 3.2 ka. Although the ages determined using the best model approach overlap, their good correspondence with those determined using the Monte Carlo approach (the youngest event at 1 ka, two events at 1.1–1.3 ka and three events at 2.1–3.2 ka with smaller slip per event values) strengthens the consistency of this set of ages.

For all events, the determined slip ranges between 0.3 and 1.2 m. Assuming that those values correspond to the maximum coseismic displacement and using the coseismic surface slip-length empirical relationships [*Manighetti et al*., 2007; *Wells and Coppersmith*, 1994], the rupture length would roughly be between 5 and 15 km. This is in agreement with morphological observations on the Pizzalto Fault that show that the fault scarp is linear and continuous over the whole 13 km long fault.

Considering a maximum surface slip between 0.3 and 1.2 m, a rupture length equal either to 5 or to 15 km, and a seismogenic width of 15 km [*Boncio et al*., 2009], we estimated the maximum magnitude of the past events recorded on the Pizzalto fault to be between $M_w = 5.9$ and $M_w = 6.6$. These estimates are in agreement with the magnitudes estimated in the region by previous studies [*Peruzza et al*., 2011; *Benedetti et al*., 2013].

7.2. Comparison With Existing Paleoseismological Records From the Rotella-Aremogna Fault System

D'Addezio et al. [2001], based on several trenches made on three segments of the Rotella-Aremogna fault system (Figure 1), concluded that all fault segments ruptured during coeval events dated between 800 B.C. and 1030 A.D. (2.8–1 ka), between 3735 B.C. and 2940 B.C. (5.7–4.9 ka), and between 3540 B.C. and 5000 B.C. (5.5–7 ka). The time range of the proposed youngest event determined by *D'Addezio et al*. [2001] overlaps with that determined for the seismic activity of the Pizzalto fault (0.8–3.2 ka). The slip associated with the last event identified by *D'Addezio et al*. [2001] ranges between 0.3 to 1 m on each segment, similar to the slip per event range determined for the Pizzalto fault (0.3–1.2 m).

The most recent seismic activity on the Pizzalto and the Aremogna-Cinque Miglia faults thus appears to have occurred during the same time period. It is, however, not possible to determine whether this period of common seismic activity corresponds to earthquakes events rupturing both faults during a single very energetic event or to a sequence of closely temporally spaced smaller events breaking each segment consecutively.

However, our results suggest that at least six events have occurred on the Pizzalto fault over a time span of ~2.4 kyr, whereas *D'Addezio et al*. [2001] identified a single event on the Aremogna-Cinque Miglia segments within a similar time period (~1.8 kyr). If the seismic activity of both fault segments is coeval, how can such a difference in the number of events be accounted for? The Aremogna-Cinque Miglia fault system is located at the southern tip of the Rotella-Aremogna fault system and is composed of several fault segments less than 5 km long. The Pizzalto fault is the most prominent fault of the system and is approximately 13 km long. It is therefore possible that some slip events that occurred on the Pizzalto fault did not rupture the Aremogna and Cinque Miglia segments, were not recorded in the trenches because their amplitude was not large enough to be detected, or were distributed among other smaller segments.

Finally, if the entire Rotella-Aremogna fault system ruptured during a single event, as suggested by *Boncio et al*., [2004], who interprets this system to be a unique seismogenic source, the expected magnitude would be up to $M_w = 6.8$. This magnitude is calculated considering a mean slip for this event of 1.2 m and a total length of 30 km, with all others parameters being similar to those used for the single Pizzalto fault. If we assume that this is the case, by extrapolating the results from *D'addezio et al*. [2001], the Aremogna-Rotella system might have experienced two periods of intense seismic activity between 0.8 and 3.2 ka and between 5 and 7 ka, separated by a quiescent period of approximately 2 kyr.

In agreement with our results suggesting that no event has occurred on this system since 0.8 ka, there are no large ($M_w > 5.5$) historical events with epicenters located near the Pizzalto fault in the CPTI11 catalogue [*Rovida et al*., 2011].

7.3. Slip Versus Time

The time period recovered by this study does not capture the full seismic cycle because the slip rate of 1.4–2.6 mm/yr determined over the whole 3.2 kyr of exposure history remains 2 to 3 times higher than the slip rates determined over longer time periods (10–15 kyr) on Apenninic faults [*Roberts and*

Michetti, 2004; *Benedetti et al*., 2013]. Those values are probably not representing the long-term slip rate of the Pizzalto fault and might suggest an increase in slip during the last 3.2 kyr associated with an intense period of seismic activity. Significant variations in the slip rate over a similar timescale have been reported for other Apenninic [*Benedetti et al*., 2013; *Schlagenhauf et al*., 2011] and worldwide faults [*Friedrich et al*., 2003; *Scholz*, 2010; *Ratzov et al*., 2015]. It is interesting to note that considering only the seismic cluster time interval, the derived slip acceleration on the Pizzalto fault (2.2–4.8 mm/yr) is similar to that derived for other faults in the central Apennines (2–10 mm/yr) [*Benedetti et al*., 2013].

7.4. Comparing the Seismic History of the Pizzalto Fault With Other Paleoseismological Records in the Central Apennines

The results obtained from four trenches dug along a 5 km long segment located approximately 20 km north of the Pizzalto fault at the northern tip of the 30 km long Sulmona fault system suggest that two large earthquakes occurred at 1.7–1.9 ka and 4.3–4.9 ka and that the associated slips were approximately 1 m [*Galli et al*., 2015]. While both the slip per event value and the age of the last event are similar to that estimated at Pizzalto, the older event apparently occurred approximately 1–2 ka earlier than that recorded by *D'Addezio et al*. [2001] on the Aremogna segment (Figure 1).

The seismic history of the San Sebastiano fault, located approximately 25 km west of the Pizzalto fault, has been assessed through ^{36}Cl exposure dating of its 4 m high fault scarp [*Benedetti et al*., 2013]. The San Sebastiano fault record suggests the occurrence of an intense period of seismic activity from 3.9 to 4.5 ka, which does not coincide with the timing of activity at Pizzalto (from 0.8 to 3.2 ka). However, the seismic history of four clustered events in less than 1 kyr and the slip per event (0.5–1.2 m) are similar to those deduced from the Pizzalto fault study. Moreover, the intracluster recurrence time is similar for both faults (200 yrs).

At a broader scale, *Benedetti et al*. [2013] have shown that the faults belonging to the Fucino South fault system (San Sebastiano, Parasano, and Trasacco), situated 25 to 45 km to the west, have ruptured with 0.2 to 1.6 m of slip per event. This is similar to the slip per event at the Pizzalto fault (0.3 to 1.2 m). The seismic activity of the Pizzalto fault approximately coincides with the last period of activity recorded at 1.5–3 ka on both the Parasano and Trasacco faults. In particular, three events have been recorded on the Parasano fault at 1.7, 2.5, and 3.0 (±0.5) ka, similarly to the Pizzalto fault. Trenches on the Serrone fault also suggest that an earthquake occurred on this fault at 2.3–2.9 ka.

Considered all together, these observations suggest that the seismic history of the Pizzalto fault is characterized by clustered events occurring during periods of intense seismic activity lasting 1 to 2 ka and is similar to the history of the Fucino South faults. In addition, the slip per event values (0.3–1.2 m) are comparable. Finally, the record from the Pizzalto fault suggests that its seismic activity coincides with activity on the Serrone and Parasano faults mapped as smaller secondary faults of the Fucino South system by *Benedetti et al*. [2013]. In contrast, the activity on the Pizzalto fault did not occur simultaneously with that on the San Sebastiano and Trasacco faults. The question arises whether these observations are indicative of a nonrandom process of earthquake occurrence, as it has long been suggested. More paleoseismological data are required to statistically strengthen these hypotheses.

7.5. Probabilistic Seismic Hazard Evaluations

If we assume a Poisson distribution of earthquakes, the only required information is the mean recurrence time and an exponential distribution describing the time intervals between events. The probability of the next earthquake occurrence is independent of the time since the last event. In fact, in a Poisson distribution, if earthquakes occur at an average rate (λ) per unit of time, there will be on average $\lambda \times w$ occurrences per w unit of time. The probability that at least one event occurs during a w equal to 50 years can be expressed as follows:

$$P(x \geq 1) = 1 - P(x = 0) = 1 - e^{\lambda \times 50} \quad (1)$$

In contrast, time-dependent models of earthquake occurrence are based on the assumption that the probability of an earthquake occurrence, in a given time period, follows a renewal model, where the stress that is released in the earthquake has built up over time. Following *Peruzza et al*. [2011], we adopted the simplest time-dependent process, namely, the renewal process, to calculate the conditional probability of an

earthquake occurrence for the Pizzalto fault using Brownian passage-time (BPT) distributions. The time elapsed since the last characteristic earthquake (T_{elap}) is used to calculate the conditional probability of an event occurring in the next 50 years:

$$P(t) = \sqrt{\frac{T_{mean}}{2\pi \times CV^2 \times t^3}}\, e^{-\frac{(t-T_{mean})}{2\times T_{mean}\times CV^2 \times t}} \quad (2)$$

$$P\left(T_{elap} \le T \le {}^{\Delta T}/_{T} > T_{elap}\right) = \frac{P\left(T_{elap} \le T \le T_{elap} + \Delta T\right)}{1 - P\left(0 \le T \le T_{elap}\right)} \quad (3)$$

where T_{mean} is the mean recurrence time (defined as the recurrence interval between similar-sized, maximum expected earthquakes from the seismogenic sources) and CV is the variation coefficient of the distribution, given by the ratio $CV = \sigma/T_{mean}$ (the standard deviation σ over the mean recurrence time) [*Visini and Pace*, 2014].

Therefore, to evaluate the Poisson probability of occurrence, we need to know T_{mean}, and to evaluate the BPT probability of occurrence, we also need CV and T_{elap}.

Considering the reconstructed seismic history of the Pizzalto fault, *n* simulations of the earthquake catalogue (hereafter synthetic catalogues) are performed with the age of each event randomly varying within their uncertainties. In total, 5000 synthetic catalogues were computed, and T_{mean}, CV, and T_{elap} were extracted from each of them. Figure 10a displays a contour plot of the T_{mean} and CV pairs for each synthetic catalogue.

The results show that the T_{mean} and CV peak at approximately 420–460 years and 0.9–1.2, respectively (Figure 10a). The resulting T_{mean} is significantly lower than the values reported in the literature, which are derived from long-term slip rates (roughly 1200 years [*Peruzza et al*., 2011]) and from paleoseismological studies (more than 2000 years [*D'Addezio et al*., 2001]). The resulting CV confirms the clustering behavior of the Pizzalto fault ($CV > 1$) and is higher than the values published by *Peruzza et al*. [2011]. In terms of the probability of occurrence within 50 years (Figure 10b), the calculated Poisson values range between 9% and 17%, whereas the time-dependent values calculated for the next 50 years range between 5% and 26%.

By repeating the experiment and including the results obtained from *D'Addezio et al*. [2001], thus assuming that the Pizzalto fault also ruptured 5–7 ka ago, this approach leads to T_{mean} and CV pairs ranging between 700–850 years and 1.0–1.4, respectively (Figure 10c). This higher T_{mean} value is in better agreement with previously published values derived from long-term slip rates, while the CV value remains similar to that determined above and is thus consistent with clustering behavior on the Pizzalto fault. In terms of the probability of occurrence within 50 years (Figure 10d), the calculated Poisson values are approximately 6%, whereas the time-dependent values calculated for the next 50 years range between 4% and 10%.

8. Conclusions

We have mapped the Pizzalto fault and the Pleistocene-Holocene deposits it affects, sampled the fault plane to analyze its ^{36}Cl + REE-Y contents and determined its seismic history over the last 3 kyr. The ^{36}Cl and REE-Y concentrations were used together to accurately constrain the number of events and the slip per event. We determined at least six earthquake events occurred over the last 3 kyr, and the presented results indicate that the Pizzalto fault is seismically active and able to generate moment magnitudes up to 6.4.

We compared the [REE-Y] and [^{36}Cl] data from the fault plane samples and demonstrated that the [REE-Y] could also be affected by the seismic exhumation process, thereby producing characteristic concentration patterns. The slip event amplitudes estimated from the analysis of both [^{36}Cl] and [REE-Y] are similar, which suggests that the use of [REE-Y] could greatly contribute to reducing the uncertainties in this parameter, especially when [^{36}Cl] profiles as a function of depth are smooth. The presented results strengthen similar observations made on the Magnola fault (Italy) by *Carcaillet et al*. [2008] and *Manighetti et al*. [2010]. While the process of [REE-Y] accumulation in the fault plane remains unclear, the first-order similarity of the concentrations observed at the Pizzalto and Magnola faults confirms that these elements can be used as a proxy of slip events. We thus recommend the use of [REE-Y] to complement [^{36}Cl] in the recovery of past earthquakes on a fault plane in order to enhance the resolution of the slip in the deduced seismic histories.

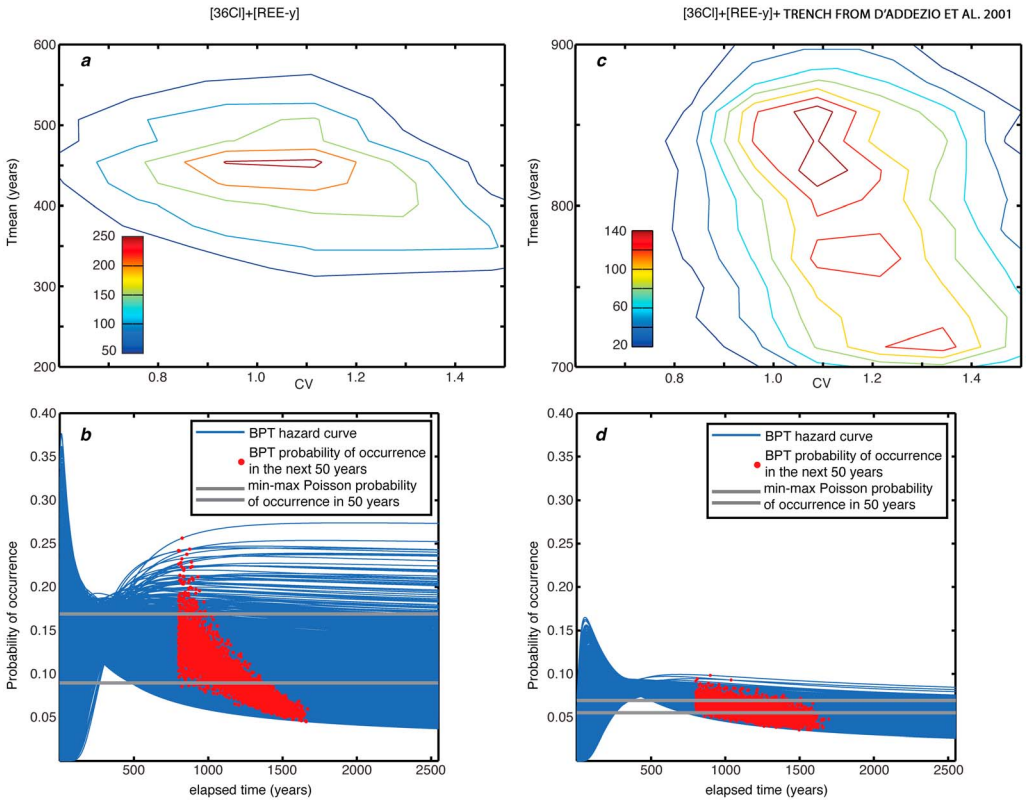

Figure 10. (a) Contour plot of 5000 pairs of T_{mean} and CV values for each synthetic catalogue obtained from our best seismic scenario. (b) Poissonian and conditional probabilities (BPT) of an earthquake occurring along the Pizzalto fault based on the input of T_{mean}, CV, and T_{elap} from each synthetic catalogue obtained from our best seismic scenario (S6). (c) Contour plot of 5000 pairs of T_{mean} and CV of each synthetic catalogue obtained from our most satisfying seismic scenario together with the trenching data from *D'Addezio et al.* [2001]. (d) Poissonian and conditional probabilities (BPT) of an earthquake occurring along the Pizzalto fault based on the input of T_{mean}, CV, and T_{elap} from each synthetic catalogue obtained from our most satisfying seismic scenario together with the trenching data from *D'Addezio et al.* [2001].

We show that the Pizzalto fault released its accumulated strain through clustered events, which appears to be a common behavior of the normal faults in the Apennines during the Holocene period [*Benedetti et al.*, 2013]. Integrating paleoseismological data from the adjacent Rotella-Aremogna fault system from *D'Addezio et al.* [2001], we model the time-dependent probability of earthquake occurrence for the next 50 years. The results indicate that the Rotella-Aremogna-Pizzalto fault system has a low to moderate probability (between 4% to 26%) of earthquake occurrence in the next 50 years.

The data presented and discussed in this work are of primary importance because of the following points:

1. This is the first time that paleoseismological data from various methods (cosmic ray exposure dating and trenches) are integrated together in a seismic hazard assessment.
2. The complementarity of these two methods enables us to recover a complete, reliable and long history of the Rotella-Aremogna-Pizzalto fault system.
3. We demonstrate that the Rotella-Aremogna fault system and the Pizzalto faults are able to rupture in the next centuries and, potentially, together. It remains unclear whether these faults are physically linked at depth or interact through stress transfer. In any case, their seismic histories show that they can be considered a single seismic source, as proposed by *Boncio et al.* [2004].
4. The Rotella-Aremogna-Pizzalto fault system has a mean recurrence time (0.8 kyr) shorter than that of the Apenninic faults (~2 kyr [*Galli et al.*, 2008]). The question of whether the classical approach in paleoseismology (trenches) used alone is able to provide a reliable T_{mean} in the Apennines must be examined. At the scale of the individual seismogenic sources defined for seismic hazard evaluations, we believe that integrating data from cosmic ray exposure dating could dramatically change the T_{mean} and CV parameters

and, hence, affect the associated probabilities of earthquake occurrence [*Peruzza et al*., 2011]. We would like to stress that it now appears important to couple these different paleoseismological methods to reconstruct accurate, long, reliable, and representative time series of earthquake occurrence. We highlight that the results provided here could be directly used to improve regional probabilistic seismic hazard models.

5. On a larger scale, we observe similarities between the seismic histories of several faults belonging to two adjacent fault systems. This might be related to nonrandom processes occurring in the release of the strain accumulated on faults, commonly referred to as fault interactions, leading to apparent synchronization, as suggested by *Scholz* [2010]. If these processes were determined to be the main parameter controlling the occurrence of earthquakes, it would be crucial to take them into account in probabilistic seismic hazard models [*Visini and Pace*, 2014].

Acknowledgments
Our work has been funded by Fondi Ateneo ex 60% (respresentative B. Pace) and MIUR funded project FIRB Abruzzo (code: RBAP10ZC8K_006). We warmly thank A. Schlagenhauf, F. Ranalli, and P. Di Federico (Pigi) for helping us in the field and D. Di Naccio for the DEM data. J. Marin and all the staff at SARM-CRPG (France) are particularly acknowledged for the chemical measurements. The ASTER French AMS national facility (CEREGE, Aix-en-Provence, France) is supported by the INSU/CNRS, the French Ministry of Research and Higher Education, IRD, and CEA. We also wish to thank Julià Garcìa-Mayordomo and an anonymous reviewer for their careful and very useful review. The data used are listed in the supplements.

References

Akaike, H. (1974), A newlook at statistical model identification, *IEEE Trans. Autom. Control*, *19*(6), 716–723.

Armijo, R., P. Tapponnier, J. L. Mercier, and T.-L. Han (1986), Quaternary extension in southern Tibet: Field observations and tectonic implications, *J. Geophys. Res.*, *91*(B14), 13,803–13,872, doi:10.1029/JB091iB14p13803.

Armijo, R., H. Lyon-Caen, and D. Papanastassiou (1992), East-west extension and Holocene normal-fault scarps in the Hellenic arc, *Geology*, *20*(6), 491–494.

Benedetti, L. (1999), Sismotectonique de l'Italie et des régions adjacentes: Fragmentation du promontoire adriatique Ph. D. Thesis, Univerisy Paris.

Benedetti, L. C., and J. van der Woerd (2014), Cosmogenic nuclide dating of earthquakes, faults, and toppled blocks, *Elements*, *10*(5), 357–361, doi:10.2113/gselements.10.5.357.

Benedetti, L., R. Finkel, D. Papanastassiou, G. King, R. Armijo, F. Ryerson, D. Farber, and F. Flerit (2002), Post-glacial slip history of the Sparta fault (Greece) determined by ^{36}Cl cosmogenic dating: Evidence for non-periodic earthquakes, *Geophys. Res. Lett.*, *29*(8), 1246, doi:10.1029/2001GL014510.

Benedetti, L., R. Finkel, G. King, R. Armijo, D. Papanastassiou, F. J. Ryerson, F. Flerit, D. Farber, and G. Stavrakyrkis (2003), Motion on the Kyrparelli fault (Greece) prior to the 1981 earthquake sequence determined from ^{36}Cl cosmogenic dating, *Terra Nova*, *15*(2), 118–124, doi:10.1046/j.1365-3121.2003.00474.x.

Benedetti, L., I. Manighetti, Y. Gaudemer, R. Finkel, J. Malavieille, K. Pou, M. Arnold, G. Aumaître, D. Bourlès, and K. Keddadouche (2013), Earthquake synchrony and clustering on Fucino faults (Central Italy) as revealed from in situ ^{36}Cl exposure dating, *J. Geophys. Res. Solid Earth*, *118*, 4948–4974, doi:10.1002/jgrb.50299.

Boncio, P., G. Lavecchia, and B. Pace (2004), Defining a model of 3D seismogenic sources for Seismic Hazard Assessment applications: The case of central Apennines (Italy), *J. Seismol.*, *8*(3), 407–425, doi:10.1023/B:JOSE.0000038449.78801.05.

Boncio, P., D. Tinari, G. Lavecchia, F. Visini, and G. Milana (2009), The instrumental seismicity of the Abruzzo Region in Central Italy (1981–2003): Seismotectonic implications, *Ital. J. Geosci.(Boll. Soc. Geol. It.)*, *128*(2), 367–380, doi:10.3301/IJG.2009.128.2.367.

Boncio, P., A. Pizzi, F. Brozzetti, G. Pomposo, G. Lavecchia, D. Di Naccio, and F. Ferrarini (2010), Coseismic ground deformation of the 6 April 2009 L'Aquila earthquake (central Italy, M_w 6.3), *Geophys. Res. Lett.*, *37*, L06308, doi:10.1029/2010GL042807.

Bosi, C. (1975), Osservazioni preliminari su faglie probabilmente attive nell'Appennino centrale, *Boll. della Soc. Geol. Ital.*, *94*(4), 827–859.

Bosi, C., F. Galadini, B. Giaccio, P. Messina, and A. Sposato (2003), Plio-Quaternary continental deposits in the Latium-Abruzzi Apennines: The correlation of geological events across different intermontane basins, *Quaternario*, *16*(1Bis), 55–76.

Braucher, R., E. T. Brown, D. L. Bourlès, and F. Colin (2003), In situ produced ^{10}Be measurements at great depths: Implications for production rates by fast muons, *Earth Planet. Sci. Lett.*, *211*(3), 251–258.

Brunamonte, F., A. M. Michetti, L. Serva, and E. Vittori (1991), Evidenze paleosismologiche nell'Appennino Centrale ed implicazioni neotettoniche, in *Studi preliminari all'acquisizione dati del profilo CROP11 Civitavecchia-Vasto*, *St. Geol. Camerti, Spec*., vol. 1991/2, edited by M. Tozzi, G. P. Cavinato, and M. Parotto, pp. 265–270, Università degli studi di Camerino, Camerino, Italy.

Burnham, K. P., and D. R. Anderson (2002), *Model Selection and Multi-Model Inference: Apractical Information-Theoretical Approach*, Springer, New York.

Carcaillet, J., I. Manighetti, C. Chauvel, A. Schlagenhauf, and J.-M. Nicole (2008), Identifying past earthquakes on an active normal fault (Magnola, Italy) from the chemical analysis of its exhumed carbonate fault plane, *Earth Planet. Sci. Lett.*, *271*(1–4), 145–158, doi:10.1016/j.epsl.2008.03.059.

Carignan, J., P. Hild, G. Mevelle, J. Morel, and D. Yeghicheyan (2001), Routine analyses of trace elements in geological samples using flow injection and low pressure on-line liquid chromatography coupled to ICP-MS: A study of geochemical reference materials BR, DR-N, UB-N, AN-G and GH, *Geostand. Newsl.*, *25*(2–3), 187–198, doi:10.1111/j.1751-908X.2001.tb00595.x.

Chiarabba, C., et al. (2009), The 2009 L'Aquila (central Italy) M_W 6.3 earthquake: Main shock and aftershocks, *Geophys. Res. Lett.*, *36*, L18308, doi:10.1029/2009GL039627.

Chiaraluce, L., M. Barchi, C. Collettini, F. Mirabella, and S. Pucci (2005), Connecting seismically active normal faults with Quaternary geological structures in a complex extensional environment: The Colfiorito 1997 case history (northern Apennines, Italy), *Tectonics*, *24*, TC1002, doi:10.1029/2004TC001627.

Civico, R., S. Pucci, P. M. De Martini, and D. Pantosti (2015), Morphotectonic analysis of the long-term surface expression of the 2009 L'Aquila earthquake fault (Central Italy) using airborne LiDAR data, *Tectonophysics*, *644–645*, 108–121, doi:10.1016/j.tecto.2014.12.024.

D'addezio, G., E. Masana, and D. Pantosti (2001), The holocene paleoseismicity of the Aremogna-Cinque Miglia Fault (Central Italy), *J. Seismol.*, *5*(2), 181–205, doi:10.1023/A:1011403408568.

D'Agostino, N., A. Avallone, D. Cheloni, E. D'Anastasio, S. Mantenuto, and G. Selvaggi (2008), Active tectonics of the Adriatic region from GPS and earthquake slip vectors, *J. Geophys. Res.*, *113*, B12413, doi:10.1029/2008JB005860.

Dia, A., G. Gruau, G. Olivié-Lauquet, C. Riou, J. Molénat, and P. Curmi (2000), The distribution of rare earth elements in groundwaters: Assessing the role of source-rock composition, redox changes and colloidal particles, *Geochim. Cosmochim. Acta*, *64*(24), 4131–4148, doi:10.1016/S0016-7037(00)00494-4.

Duddy, L. R. (1980), Redistribution and fractionation of rare-earth and other elements in a weathering profile, *Chem. Geol.*, *30*(4), 363–381, doi:10.1016/0009-2541(80)90102-3.
Field, E. H., et al. (2014), Uniform California Earthquake Rupture Forecast, Version 3 (UCERF3)—The time-independent model, *Bull. Seismol. Soc. Am.*, *104*(3), 1122–1180, doi:10.1785/0120130164.
Field, E. H., et al. (2015), Long-term time-dependent probabilities for the Third Uniform California Earthquake Rupture Forecast (UCERF3), *Bull. Seismol. Soc. Am.*, *105*(2), 511–543, doi:10.1785/0120140093.
Fierer, N., A. S. Allen, J. P. Schimel, and P. A. Holden (2003), Controls on microbial CO_2 production: A comparison of surface and subsurface soil horizons, *Global Chang. Biol.*, *9*(9), 1322–1332, doi:10.1046/j.1365-2486.2003.00663.x.
Fifield, L. K., T. R. Ophel, G. L. Allan, J. R. Bird, and R. F. Davie (1990), Accelerator mass spectrometry at the Australian National University's 14UD accelerator: Experience and developments, in *Nuclear Instruments & Methods in Physics Research, Section B (Beam Interactions with Materials and Atoms)*, *Dept. of Nucl. Phys.*, vol. B52, pp. 233–237, Australian Nat. Univ, Canberra, ACT, Australia.
Frezzotti, M., and C. Giraudi (1989), L'evoluzione geologica tardo-pleistocenica ed olocenica del Piano di Aremogna (Roccaraso-Abruzzo): Implicazioni climatiche e tettoniche, *Memorie Società Geologica Italiana*, *42*, 5–19.
Friedrich, A. M., B. P. Wernicke, N. A. Niemi, R. A. Bennett, and J. L. Davis (2003), Comparison of geodetic and geologic data from the Wasatch region, Utah, and implications for the spectral character of Earth deformation at periods of 10 to 10 million years, *J. Geophys. Res.*, *108*(B4), 2199, doi:10.1029/2001JB000682.
Galadini, F., and P. Galli (2000), Active tectonics in the central Apennines (Italy)—Input data for seismic hazard assessment, *Nat. Hazards*, *22*, 225–270, doi:10.1023/A:1008149531980.
Galli, P., F. Galadini, and D. Pantosti (2008), Twenty years of paleoseismology in Italy, *Earth Sci. Rev.*, *88*(1–2), 89–117, doi:10.1016/j.earscirev.2008.01.001.
Galli, P., B. Giaccio, E. Peronace, and P. Messina (2015), Holocene paleoearthquakes and early-late Pleistocene slip rate on the Sulmona fault (central Apeninnes, Italy), *Bull. Seismol. Soc. Am.*, *105*(1), 1–13, doi:10.1785/0120140029.
Giraudi, C. (1995), Considerations on the significance of some post-glacial fault scarps in the Abruzzo Apennines (Central Italy), *Quat. Int.*, *25*(94), 33–45, doi:10.1016/1040-6182(94)00033-2.
Gosse, J. C., and F. M. Phillips (2001), Terrestrial in situ cosmogenic nuclides: Theory and application, *Quat. Sci. Rev.*, *20*, 1475–1560.
Kase, Y. (2010), Slip-length scaling law for strike-slip multiple segment earthquakes based on dynamic rupture simulations, *Bull. Seismol. Soc. Am.*, *100*(2), 473–481, doi:10.1785/0120090090.
Lavecchia, G., F. Brozzetti, M. Barchi, M. Menichetti, and J. V. A. Keller (1994), Seismotectonic zoning in east-central Italy deduced from an analysis of the Neogene to present deformations and related stress fields, *Geol. Soc. Am. Bull.*, *106*(9), 1107–1120, doi:10.1130/0016-7606(1994)106<1107:SZIECI>2.3.CO;2.
Lowell, T. V. (1995), The application of radiocarbon age estimates to the dating of glacial sequences: An example from the Miami sublobe, Ohio, U.S.A, *Quat. Sci. Rev.*, *14*(1), 85–99, doi:10.1016/0277-3791(94)00113-P.
Manighetti, I., M. Campillo, S. Bouley, and F. Cotton (2007), Earthquake scaling, fault segmentation, and structural maturity, *Earth Planet. Sci. Lett.*, *253*(3–4), 429–438, doi:10.1016/j.epsl.2006.11.004.
Manighetti, I., E. Boucher, C. Chauvel, A. Schlagenhauf, and L. Benedetti (2010), Rare earth elements record past earthquakes on exhumed limestone fault planes, *Terra Nova*, *22*(6), 477–482, doi:10.1111/j.1365-3121.2010.00969.x.
Manighetti, I., C. Caulet, D. De Barros, C. Perrin, F. Cappa, and Y. Gaudemer (2015), Generic along-strike segmentation of Afar normal faults, East Africa: Implications on fault growth and stress heterogeneity on seismogenic fault planes, *Geochem. Geophys. Geosyst.*, *16*, 443–467, doi:10.1002/2014GC005691.
Miccadei, E., and M. Parotto (1998), Assetto geologico delle dorsali Rotella-Pizzalto-Porrara (Appennino abruzzese orientale), *Geol. Rom.*, *34*, 87–113.
Mitchell, S. G., A. Matmon, P. R. Bierman, Y. Enzel, M. Caffee, and D. Rizzo (2001), Displacement history of a limestone normal fault scarp, northern Israel, from cosmogenic Cl-36, *J. Geophys. Res.*, *106*(B3), 4247–4264, doi:10.1029/2000JB900373.
Moraetis, D., V. Mouslopoulou, and A. Pratikakis (2015), Sorption of the Rare Earth Elements and Yttrium (REE-Y) in calcite: The mechanism of a new effective tool in identifying paleoearthquakes on carbonate faults in *E.G.U 2015*.
Mouslopoulou, V., A. Nicol, J. J. Walsh, J. G. Begg, D. B. Townsend, and D. T. Hristopulos (2012), Fault-slip accumulation in an active rift over thousands to millions of years and the importance of paleoearthquake sampling, *J. Struct. Geol.*, *36*, 71–80, doi:10.1016/j.jsg.2011.11.010.
Pace, B., L. Peruzza, G. Lavecchia, and P. Boncio (2006), Layered seismogenic source model and probabilistic seismic-hazard analyses in Central Italy, *Bull. Seismol. Soc. Am.*, *96*(1), 107–132, doi:10.1785/0120040231.
Pace, B., P. Boncio, and G. Lavecchia (2002), The 1984 Abruzzo earthquake (Italy): An example of seismogenic process controlled by interaction between differently oriented synkinematic faults, *Tectonophysics*, *350*(3), 237–254, doi:10.1016/S0040-1951(02)00118-X.
Pace, B., F. Visini, and L. Peruzza (2016), FiSH: MATLAB tools to turn fault data into seismic hazard models, *Seismol. Res. Lett.*, 87–2A, doi:10.1785/0220150189.
Palumbo, L., L. Benedetti, D. Bourlès, A. Cinque, and R. Finkel (2004), Slip history of the Magnola fault (Apennines, Central Italy) from ^{36}Cl surface exposure dating: Evidence for strong earthquakes over the Holocene, *Earth Planet. Sci. Lett.*, *225*(1–2), 163–176, doi:10.1016/j.epsl.2004.06.012.
Papanikolaou, I. D., and G. P. Roberts (2007), Geometry, kinematics and deformation rates along the active normal fault system in the southern Apennines: Implications for fault growth, *J. Struct. Geol.*, *29*(1), 166–188, doi:10.1016/j.jsg.2006.07.009.
Paul, E. A., and F. E. Clark (1989), *Soil Microbiology and Biochemistry*, Academic Press, New York.
Peruzza, L., D. Pantosti, D. Slejko, and G. Valensise (1997), Testing a new hybrid approach to seismic hazard assessment: An application to the Calabrian Arc (Southern Italy), *Nat. Hazards*, *14*(2–3), 113–126, doi:10.1007/BF00128260.
Peruzza, L., B. Pace, and F. Visini (2011), Fault-based earthquake rupture forecast in Central Italy: Remarks after the L'Aquila M_w 6.3 Event, *Bull. Seismol. Soc. Am.*, *101*(1), 404–412, doi:10.1785/0120090276.
Piccardi, L., Y. Gaudemer, P. Tapponnier, and M. Boccaletti (1999), Active oblique extension in the central Apennines (Italy): Evidence from the Fucino region, *Geophys. J. Int.*, *139*(2), 499–530, doi:10.1046/j.1365-246x.1999.00955.x.
Pingue, F., G. De Natale, and P. Briole (1993), Modeling of the 1980 Irpinia earthquake source: Constraints from geodetic data, *Ann. Geofis.*, *36*(1), 27–39.
Plan, L. (2005), Factors controlling carbonate dissolution rates quantified in a field test in the Austrian alps, *Geomorphology*, *68*(3–4), 201–212, doi:10.1016/j.geomorph.2004.11.014.
Pondrelli, S., S. Salimbeni, G. Ekström, A. Morelli, P. Gasperini, and G. Vannucci (2006), The Italian CMT dataset from 1977 to the present, *Phys. Earth Planet. Inter.*, *159*(3–4), 286–303, doi:10.1016/j.pepi.2006.07.008.
Pourret, O., M. Davranche, G. Gruau, and A. Dia (2007), Organic complexation of rare earth elements in natural waters: Evaluating model calculations from ultrafiltration data, *Geochim. Cosmochim. Acta*, *71*(11), 2718–2735, doi:10.1016/j.gca.2007.04.001.

Pucci, S., F. Villani, R. Civico, D. Pantosti, P. Del Carlo, A. Smedile, P. M. De Martini, E. Pons-Branchu, and A. Gueli (2015), Quaternary geology of the Middle Aterno Valley, 2009 L'Aquila earthquake area (Abruzzi Apennines, Italy), *J. Maps*, *11*(5), 689–697.

Ratzov, G., A. Cattaneo, N. Babonneau, J. Déverchère, K. Yelles, R. Bracene, and F. Courboulex (2015), Holocene turbidites record earthquake supercycles at a slow-rate plate boundary, *Geology*, *43–4*, 331–334, doi:10.1130/G36170.1.

Reardon, E. J., G. B. Allison, and P. Fritz (1979), Seasonal chemical and isotopic variations of soil CO_2 at Trout Creek, Ontario, *Dev. Water Sci.*, *12*(C), 355–371, doi:10.1016/S0167-5648(09)70026-7.

Roberts, G. P., and A. M. Michetti (2004), Spatial and temporal variations in growth rates along active normal fault systems: An example from The Lazio–Abruzzo Apennines, central Italy, *J. Struct. Geol.*, *26*(2), 339–376, doi:10.1016/S0191-8141(03)00103-2.

Rovida, A., R. Camassi, P. Gasperini, and M. Stucchi (Eds.) (2011), *CPTI11, the 2011 Version of the Parametric Catalogue of Italian Earthquakes*, Milano, Bologna, http://emidius.mi.ingv.it/CPTI, doi:10.6092/INGV.IT-CPTI11.

Schimmelpfennig, I., et al. (2009), Sources of in-situ ^{36}Cl in basaltic rocks. Implications for calibration of production rates, *Quat. Geochronol.*, *4*(6), 441–461.

Schimmelpfennig, I., L. Benedetti, V. Garreta, R. Pik, P. Blard, P. Burnard, D. Bourlès, R. Finkel, K. Ammon, and T. Dunai (2011), Calibration of cosmogenic ^{36}Cl production rates from Ca and K spallation in lava flows from Mt. Etna (38°N, Italy) and Payun Matru (36°S, Argentina), *Geochim. Cosmochim. Acta*, *75*(10), 2611–2632, doi:10.1016/j.gca.2011.02.013.

Schlagenhauf, A., Y. Gaudemer, L. Benedetti, I. Manighetti, L. Palumbo, I. Schimmelpfennig, R. Finkel, and K. Pou (2010), Using in situ Chlorine-36 cosmonuclide to recover past earthquake histories on limestone normal fault scarps: A reappraisal of methodology and interpretations, *Geophys. J. Int.*, *182*(1), 36–72, doi:10.1111/j.1365-246X.2010.04622.x.

Schlagenhauf, A., I. Manighetti, L. Benedetti, Y. Gaudemer, R. Finkel, J. Malavieille, and K. Pou (2011), Earthquake supercycles in Central Italy, inferred from ^{36}Cl exposure dating, *Earth Planet. Sci. Lett.*, *307*(3–4), 487–500, doi:10.1016/j.epsl.2011.05.022.

Scholz, C. H. (2010), Large earthquake triggering, clustering, and the synchronization of faults, *Bull. Seismol. Soc. Am.*, *100*(3), 901–909, doi:10.1785/0120090309.

Serva, L., A. M. Blumetti, and A. Michetti (1989), Gli effetti sul terreno del terremoto del Fucino (13 gennaio 1915); tentative di interpretazione della evoluzione tettonica recente di alcune strutture, *Memorie Società Geologica Italiana*, *35*, 893–907.

Sharma, P., P. W. Kubik, U. Fehn, H. E. Gove, K. Nishiizumi, and D. Elmore (1990), Development of 36Cl standards for AMS, *Nucl. Instrum. Methods Phys. Res. Sect. B*, *52*(3–4), 410–415, doi:10.1016/0168-583X(90)90447-3.

Smith, B. J., P. A. Warke, and C. A. Moses (2000), Limestone weathering in contemporary arid environments: A case study from southern Tunisia, *Earth Surf. Process. Landforms*, *25*(12), 1343–1354, doi:10.1002/1096-9837(200011)25:12<1343::AID-ESP142>3.0.CO;2-2.

Song, Z. L., C. Q. Liu, G. L. Han, Z. L. Wang, Z. Z. Zhu, and C. Yang (2006), Enrichment and release of rare earth elements during weathering of sedimentary rocks in Wujiang Catchments, Southwest China, *J. Rare Earths*, *24*, 491–496.

Stone, J. O. (2000), Air pressure and cosmogenic isotope production, *J. Geophys. Res.*, *105*(B10), 23,753–23,759, doi:10.1029/2000JB900181.

Sweeting, M. M. (1966), The weathering of limestones, with particular reference to the Carboniferous Limestones of northern England, *Essays Geomorphol.*, 177–210.

Tarquini, S., I. Isola, M. Favalli, F. Mazzarini, M. Bisson, M. T. Pareschi, and E. Boschi (2007), TINITALY/01: A new Triangular Irregular Network of Italy, *Ann. Geophys.*, *50*, 407–425.

Taunton, A. E., S. A. Welch, and J. F. Banfield (2000), Microbial controls on phosphate and lanthanide distributions during granite weathering and soil formation, *Chem. Geol.*, *169*(3–4), 371–382, doi:10.1016/S0009-2541(00)00215-1.

Troise, C., G. De Natale, F. Pingue, and S. M. Petrazzuoli (1998), Evidence for static stress interaction among earthquakes in the south-central Apennines (Italy), *Geophys. J. Int.*, *134*(3), 809–817, doi:10.1046/j.1365-246x.1998.00610.x.

Trudgill, S. (1985), *Limestone Geomorphology*, John Wiley, New York.

Tyler, G. (2004), Rare earth elements in soil and plant systems—A review, *Plant Soil*, *267*(1–2), 191–206, doi:10.1007/s11104-005-4888-2.

Visini, F., and B. Pace (2014), Insights on a Key Parameter of Earthquake Forecasting, the Coefficient of Variation of the Recurrence Time, Using a Simple Earthquake Simulator, *Seismol. Res. Lett.*, *85*(3), 703–713, doi:10.1785/0220130165.

Wallace, R. E. (1977), Profiles and ages of young fault scarps, north-central Nevada, *Bull. Geol. Soc. Am.*, *88*(70905), 1267–1281.

Wallace, R. E. (1987), Grouping and migration of surface faulting and variations in slip rates on faults in the Great Basin province, *Bull. Seismol. Soc. Am.*, *77*(June), 868–876.

Weldon, R., K. Scharer, T. Fumal, and G. Biasi (2004), Wrightwood and the earthquake cycle: What a long recurrence record tells us about how faults work, *GSA Today*, *14*(9), 4–10.

Wells, D. L., and K. J. Coppersmith (1994), New empirical relationships among magnitude, rupture length, rupture width, rupture area, and surface displacement, *Bull. Seismol. Soc. Am.*, *84*(4), 974–1002.